3-10-2010

# Numerical Investigation of Pre-detonator Geometries for PDE Applications

Robert T. Fievisohn

# NUMERICAL INVESTIGATION OF PRE-DETONATOR GEOMETRIES FOR PDE APPLICATIONS

THESIS

Robert T. Fievisohn, 2 Lt, USAF

AFIT/GAE/ENY/10-M09

## DEPARTMENT OF THE AIR FORCE
## AIR UNIVERSITY

# *AIR FORCE INSTITUTE OF TECHNOLOGY*

**Wright-Patterson Air Force Base, Ohio**

APPROVED FOR PUBLIC RELEASE; DISTRIBUTION UNLIMITED

The views expressed in this thesis are those of the author and do not reflect the official policy or position of the United States Air Force, Department of Defense, or the United States Government. This material is declared a work of the U.S. Government and is not subject to copyright protection in the United States.

AFIT/GAE/ENY/10-M09

# NUMERICAL INVESTIGATION OF PRE-DETONATOR GEOMETRIES FOR PDE APPLICATIONS

THESIS

Presented to the Faculty

Department of Aeronautics and Astronautics

Graduate School of Engineering and Management

Air Force Institute of Technology

Air University

Air Education and Training Command

In Partial Fulfillment of the Requirements for the

Degree of Master of Science in Aeronautical Engineering

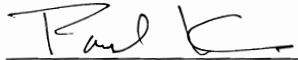Robert T. Fievisohn, B.S.

2 Lt, USAF

March, 2010

APPROVED FOR PUBLIC RELEASE; DISTRIBUTION UNLIMITED

# NUMERICAL INVESTIGATION OF PRE-DETONATOR
# GEOMETRIES FOR PDE APPLICATIONS

Robert T. Fievisohn, B.S.
2 Lt, USAF

Approved:

_____                    22 Mar 10
Dr. Paul King (Chairman)                     Date

_____                    22 Mar 2010
Maj Andrew Lofthouse (Member)                Date

_____                    22 Mar 2010
Dr. Frederick Schauer (Member)               Date

# Abstract

A parametric study was performed to determine optimal geometries to allow the successful transition of a detonation from a pre-detonator into the thrust tube of a pulse detonation engine. The study was performed using a two-dimensional Euler solver with progress variables to model the chemistry. The geometrical configurations for the simulations look at the effect of shock reflections, flow obstructions, and detonation diffraction to determine successful geometries. It was observed that there are success and failure rates associated with pre-detonators. These success rates appear to be determined by the transverse wave structure of a stably propagating detonation wave and must be considered in the design and testing of a practical pre-detonator. A simple and straight forward method of estimating the success rate is presented. Desirable effects from geometries with high success rates are used as a basis for recommendations for future pre-detonator designs.

# Acknowledgements

# Table of Contents

# List of Figures

ix

x

# List of Tables

# List of Symbols

*Acronyms*

| | |
|---|---|
| AFIT | Air Force Institute of Technology |
| AFRL | Air Force Research Laboratory |
| CJ | Chapman-Jouget |
| CFD | Computational Fluid Dynamics |
| DDT | Deflagration to detonation transition |
| FCT | Flux Corrected Transport |
| PDE | Pulse detonation engine |
| ZND | Zeldovich, von Neumann, and Döring |

*Symbols*

| | |
|---|---|
| $a_\infty$ | Freestream speed of sound |
| $c$ | Inverse freestream speed of sound |
| $c_p$ | Specific heat capacity at constant pressure |
| $d$ | Distance from expansion |
| $d_x$ | Damping coefficient in $x$-direction |
| $d_y$ | Damping coefficient in $y$-direction |
| $E$ | Energy |
| $E$ | Expansion ratio $(L/l)$ |
| $E$ | Flux vector in $x$-direction |
| $E_1, E_2$ | Activation energy |
| $F$ | Flux vector in $y$-direction |
| $h$ | Flat plate height |
| $H$ | Vector of source terms |
| $k_1, k_2$ | Pre-exponential factors |
| $l$ | Pre-detonator height |
| $L$ | Thrust tube height |
| $L^*$ | Induction length |
| $\dot{m}$ | Mass flux |
| $M$ | Mach number |
| $N_Y$ | Number of species |
| $p$ | Pressure |
| $q$ | Heat release |
| $Q$ | Vector of conserved variables |
| $R$ | Specific gas constant |
| $t$ | Time |
| $T$ | Temperature |
| $u$ | Velocity in $x$-direction |
| $v$ | Velocity in $y$-direction |

| | |
|---|---|
| $v_d$ | Velocity of detonation wave |
| $w$ | Velocity in wave-fixed frame |
| $Y_i$ | Mass fraction of species $i$ |

## *Greek*

| | |
|---|---|
| $\alpha$ | Progress variable for induction process |
| $\beta$ | Progress variable for heat release process |
| $\delta$ | Anti-diffusive flux |
| $\eta$ | Sonic parameter |
| $\eta_x$ | Diffustion coefficient in $x$-direction |
| $\eta_y$ | Diffustion coefficient in $y$-direction |
| $\gamma$ | Ratio of specific heats |
| $\lambda$ | Detonation cell width |
| $\Omega_i$ | Rate of change of species $i$ |
| $\rho$ | Density |
| $\dot{\sigma}$ | Thermicity |
| $\tau_{ind}$ | Induction time |

# NUMERICAL INVESTIGATION OF PRE-DETONATOR
# GEOMETRIES FOR PDE APPLICATIONS

## I. Introduction

A detonation is defined as a combustion wave that travels at a velocity greater than the local speed of sound of the premixed fuel/oxidizer mixture that it propagates through. The history of detonation phenomena has its start in the 1800s. The first theories were developed seperately by Chapman and Jouget in 1899 and 1905 [1]. Both developed a method to predict the wave speed of a detonation wave from only thermodynamic and hydrodynamic considerations. Measured wave speeds predicted by CJ theory match remarkably well with experimental evidence. In the 1940s, the first models for the structure of a detonation wave were put forward independently by Zeldovich, von Nuemann, and Döring. The Zeldovich, von Nuemann, and Döring (ZND) model represents the detonation as a planar shock wave followed by a reaction zone [2]. The ZND model is unstable and is only observed under transient condtions [2], however. Experimental observations show the structure of a detonation is highly three-dimensional with a cellular structure [3]. With more powerful computers being developed, accurate simulations of transient detonation waves are now becoming possible.

One of the most important applications of numerically simulating a detonation wave is the development of pulse detonation engines. A simple pulse detonation engine is a tube closed off at one end and open at the other. The tube is filled with a fuel/oxidizer mixture and then a detonation is initiated at the closed end. Then the

1

detonation wave propagates down the tube and the high pressure products created by the passing detonation wave exit the tube, generating thrust. The three phases are known as fill, detonate, and purge and are illustrated in Fig. 1.
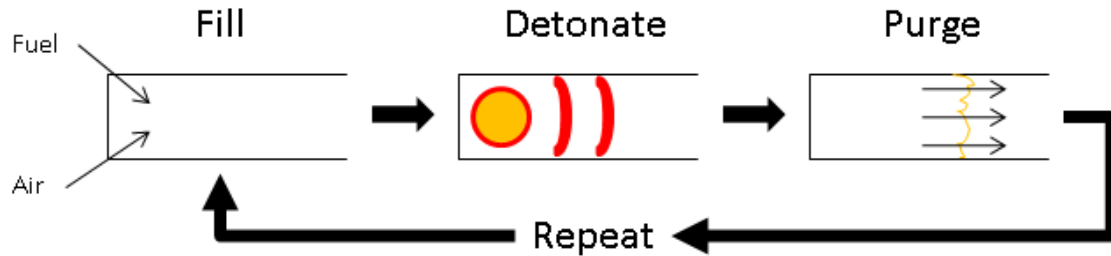


Figure 1. Conceptual pulsed detonation engine cycle.

Research [4] into air breathing pulse detonation engines has shown that these engines have the potential to be an efficient and low cost propulsion system. A pulse detonation engine (PDE) has few moving parts, high thrust, and low weight. PDEs also have the capability of operating from static to hypersonic speeds while maintaining efficiencies competitive with more conventional engines. A PDE utilizes a near constant volume heat addition and does not require a compression cycle, which leads to a simple design that is low cost, with high efficiencies and specific impulse. Before PDEs become practical there are many technological hurdles that must be overcome. One of the most important hurdles is detonation initiation and is the main focus of this research.

**Motivation**

There are several ways to initiate a detonation. First, a detonation can be directly initiated with a large enough input of energy. The amount of energy required is generally too high to be a practical solution for any type of real application [5]. The second way to initiate a detonation is to cause deflagration to detonation transition (DDT). In DDT, a fuel/oxidizer mixture is ignited, a deflagration wave forms, and

2

as it travels down the tube it will eventually transition into a detonation. Transition to detonation can be achieved more rapidly when obstructions are introduced to the travelling deflagration wave, such as a Shchelkin spiral. A third way is to use a prior detonation wave from a smaller tube to directly initiate the detonation in a larger tube (thrust tube). The smaller tube can be a crossover tube in a branched PDE setup or a pre-detonator. A pre-detonator is a device (generally a smaller tube than the thrust tube) that already has a detonation wave travelling through it. It is connected to the thrust tube and is responsible for directly initiating a detonation. The idea is that initiating a detonation in the pre-detonator requires less energy than initiation in the main tube.

PDE thrust is proportional to detonation frequency [4]. If DDT generates the detonation, increased transition time increases the detonation phase, thereby lowering the frequency and decreasing thrust. Additionally, DDT decreases engine fuel efficiency. DDT obstacle drag can decrease the fuel specific impulse by as much as 50% [6, 7]. Direct initiation from a pre-detonator can remove these losses, allowing for a higher thrust-to-weight and more fuel efficient PDE.

Current pre-detonators use fuel/oxygen mixtures. Ideally, a pre-detonator must run on fuel/air mixtures to become a practical alternative to DDT devices. Unfortunately, fuel/air mixtures require large pre-detonators because of the way a detonation diffracts from a smaller tube to a larger one. The development of practical fuel/air pre-detonators must focus on successfully using smaller diameters. Research presented in this thesis is focused on geometrical designs that have the potential to decrease pre-detonator size; allowing for the creation of the first practical pre-detonators for use in a PDE.

**Approach**

The goal of this research is to design an effective and practical pre-detonator. To accomplish this goal, a computational fluid dynamics (CFD) code is used to run parametric studies of various pre-detonator geometries. The original code was written by Dr. Viswanath R. Katta of Innovative Scientific Solutions and is known as DETON-2D [8]. A new version of the code, written in FORTRAN 90, was developed by the author to increase computational speed and add the ability to patch in two-dimensional solutions. The benefits of using this code is the short computation time (1/2 to 6 hours) required to return a solution on a single processor while still providing an accurate representation of the detonation physics. A Python script was also written to distribute multiple jobs among multiple processors; thereby allowing parametric design studies to be accomplished in a short time.

The two main geometrical configurations studied were a symmetric step expansion with a flat plate obstruction and a corner reflector. Examples of these configurations are given in Figs. 2a and 2b. It was determined that certain configurations have a



(a) Symmetric Step Expansion      (b) Corner Reflection
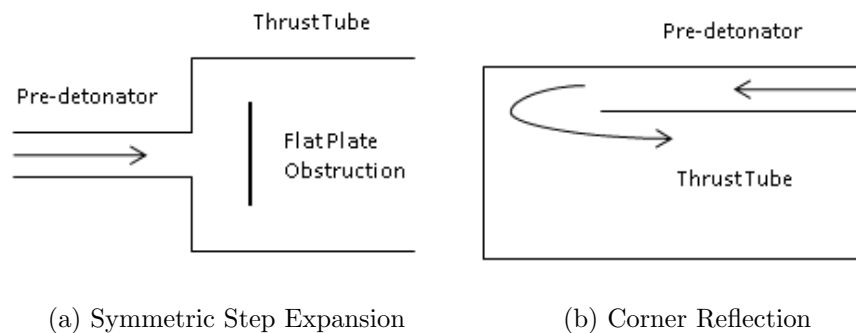
Figure 2. Main geometrical configurations studies.

probability of success or failure that is dependent upon the transverse wave structure of a detonation relative to the exit of the pre-detonator. A method for estimating success rates is developed and presented in this thesis.

4

**Organization**

The introduction has layed the framework of this research and the motivation behind it. Chapter II provides background on PDE performance as well as an overview of previous and current pre-detonator research. Chapter III goes over the theory behind detonation phenomena. Chapter IV provides details about DETON-2D. An overview of the geometrical configurations and the parametric study is given in Chapter V. Chapter V also presents the methodology to determine the success rates for the pre-detonators. Results are located in Chapter VI. Lastly, Chapter VII is composed of the conclusions and recommendations for future work.

## II.  Background

The main goal of this research is to use compuational modeling of detonation waves to aid in the design of pre-detonators for pulse detonation engines. There are many concepts, as well as design guidelines and methods that are believed to be essential in successful pre-detonator designs. Lastly, a basic overview of the parameters that govern PDE performance is given so that the role of a pre-detonator in a PDE may be better understood.

### Pre-detonator Concepts

A pre-detonator directly initiates a detonation in a thrust tube; thereby removing the need for a DDT device. The advantages are increased thrust and efficiency. Practical pre-detonators have not been developed since it is difficult to make a detonation survive while diffracting from one geometry to the other, however. Studies [9, 10] have been done with the same fuel/oxidizer mixture in both the pre-detonator and thrust tube, while others [6, 11] use different, more detonable mixtures in the pre-detonator. The effect of transitioning a detonation from an abrupt expansion [10] as well as transitioning through slowly varying expansions [9] has also been examined. Shock focusing devices and blockages in the flow [12] have been the subject of research as well.

Detonation diffraction studies are applicable to pre-detonators. Studies in the literature focus on transitioning a detonation from a small tube into an unconstrained space. Experimental evidence has shows there is a critical diameter based on the width of a detonation cell. If the tube is larger than the critical diameter, a detonation will successfully propagate into an unconstrained area. For circular channels, a critical tube diameter of 13 detonation cell widths is sufficient. Rectangular channel with an aspect ratio of one require 10 cell widths. Increasing the aspect ratio reduces the

critical diameter from 10 down to 3 for an infinite aspect ratio channel [9]. In addition to transitions into unconstrained areas, research [10] has been done on constrained areas as well. For initial diameters less than the critical diameter, the expansion ratio that a detonation can survive is dependent on the ratio of critical diameter to the initial diameter. As this ratio approachs 1, the expansion ratio a detonation can survive increases to 5. Larger ratios are considered equivalent to transitioning into an unconfined area [10]. All of the studies described above used highly sensitive mixtures such as acetylene/oxygen and hydrogen/oxygen that are easy to detonate and have small cell widths.

Practical fuel/oxidizer mixtures, such as kerosene-based fuels with air, have large cell widths. A pre-detonator using these mixtures with a diameter of 13, 10 , or even 3 cell widths is impractical because of the large size required. Experimental work [11] has been done using a sensitive fuel/oxidizer mixture in the small tube (to decrease critical diameter) and using that detonation to initiate a detonation in a large tube with a less sensitive mixture. A major drawback of this approach is the need to use oxygen instead of air. Outside of a laboratory setup it would be difficult to store or generate oxygen [6].

Instead of an abrupt expansion, a detonation could be transitioned into a larger tube using a diverging channel. Research [9] has shown that the critical diameter for increasing divergent angle increases until the angle is greater than 55 degrees. Beyond 55 degrees, the same behavior is similar to abrupt expansions. With diameters of only a few cell widths, the divergent angle a detonation can survive is only between 10 and 20 degrees. The downside to this approach is the increased length of the pre-detonator.

Research [12] that specifically studied detonation diffraction for applications to pre-detonators has also been conducted. The research aim was to find guidelines to

7

designing successful pre-detonators. The designs studied attempted to reduce the critical diameter by overdriving the detonation. An overdriven detonation decreases the cell width, thereby reducing the critical diameter requried for a successful transition. Additionaly, the use of shock focusing obstacles (cylindrical cones) were investigated. It was concluded that they were helpful but not necessary in transitioning the detonation. Another study [13] showed that a circular blockage (creating an annular geometry) at the exit of the pre-detonator enhances transmission.

Another area of pre-detonator research is using an implosion to initiate a detonation. A torodial initiator using an implosion is given in Ref. [14]. It transitions detonations around a thrust tube that converge in the center; creating a high pressure, high temperature region that produces an overdriven detonation wave. However, this initiator still uses a sensitive mixture in the pre-detonator to set off an insensitive mixture in the thrust tube.

**PDE Performance Parameters**

There are many parameters that characterize the performance of a PDE. One important characteristic is the thrust. If an engine can produce more thrust for a given size, its thrust-to-weight ratio is increased. Another important parameter is the fuel specific impluse (ISP). The ISP measures the amount of fuel required for a given change in momentum. The higher the ISP, the less fuel requried for a given change in momentum. Therefore, higher values represent more efficient engines. Both the thrust and ISP can be increased by using a pre-detonator instead of a DDT device.

The thrust and fuel specific impulse are affected by many factors. Some of these factors are cycle frequency, ignition delay, fill fraction, purge fraction, equivalence ratio, and the initiation mechanism. Cycle frequency is the number of times a PDE pulses each second. Ignition delay is the time between the end of the fill phase and

8

when the fuel ignites. The fill fraction is the percent of the tube that is filled with a combustible mixture before a detonation is set off and the purge fraction is the percentage of the tube that is filled with purge air at the end of the cycle. The initiation mechanism can be either DDT or a pre-detonator. Each of these factors can impact the performance of a PDE.

Thrust increases linearly with cycle frequency as shown in Fig. 3a. Also, Fig. 3b shows that there exists an optimal value of the ignition delay that will maximize thrust. The increase of thrust with cycle frequency is expected because the more fuel that is being burned, the more thrust that is generated. The variation in thrust with ignition delay is due to the expansion and compression waves generated during the fill phase. The detonability of a mixture is sensitive to the pressure and higher pressures require less energy to detonate. The low spots in the the thrust are when a detonation is ignited in the presense of an expansion wave and the high spots result from ignition in a compression wave [4].



| (a) | (b) |
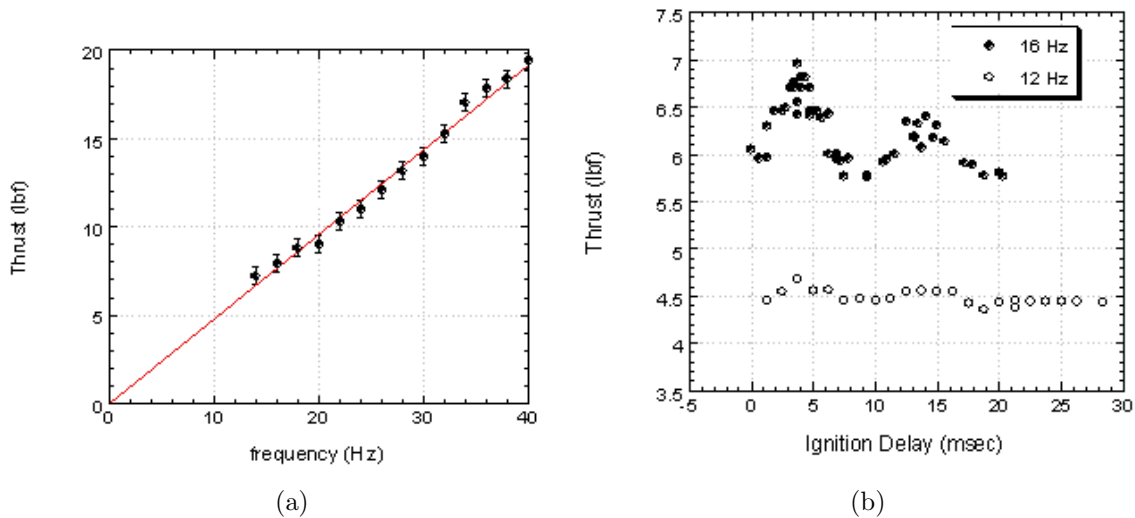
Figure 3. Impact of frequency and ignition delay on thrust. Data from [4].

Fill fraction affects both the thrust and ISP as shown in Fig. 4. Interestingly, at fill fractions around 0.3, half of the maximum thrust is still obtained while efficiency

9

has been doubled. This is because purge air being pumped by the detonation products results in a higher mass/lower $\Delta V$ [4]. Equivalence ratio also affects thrust and ISP as shown in Fig. 5.



(a)



(b)
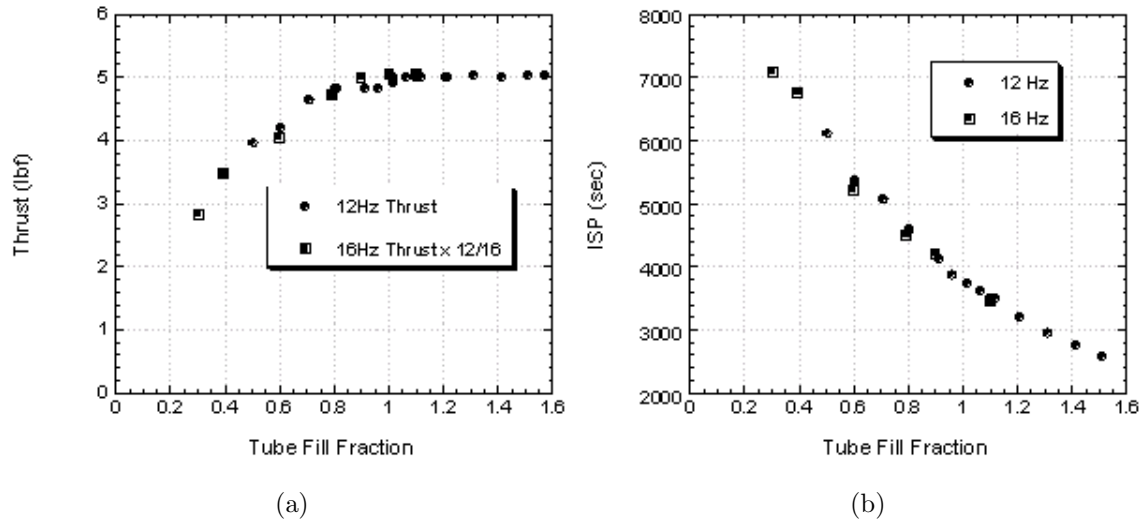
Figure 4. Impact of fill fraction on thrust and ISP. Data from [4].



(a)



(b)
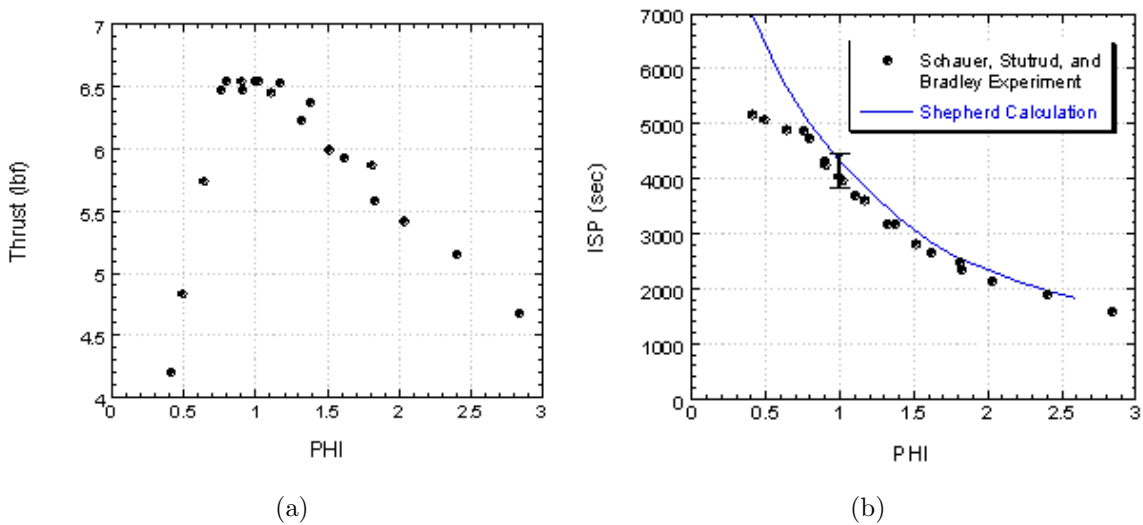
Figure 5. Effect of equivalence ratio on thrust and ISP. Data from [4].

Research [6, 7] has been done directly comparing DDT mechanisms to a pre-detonator as they relate to thrust and specific fuel impulse. A variety of DDT mecha-

10

nisms have been tested and compared to a pre-detonator which used a highly sensitive mixture. The first studies [7] examined the length of the DDT mechanism and its effect on the efficiency of the PDE. Increasing the length of the PDE is found to decrease the efficiency of the engine as shown in Fig. 6. The decrease in efficiency is due to the drag imposed by the DDT device during the blow down process. A direct comparison of a $2''$ and $3.5''$ tube initiated with a pre-detonator or a $16''$ spiral is shown in Table 1. A pre-detonator gives higher thrust and efficiency, but the need to use an oxider other than air makes pre-detonators impractical.
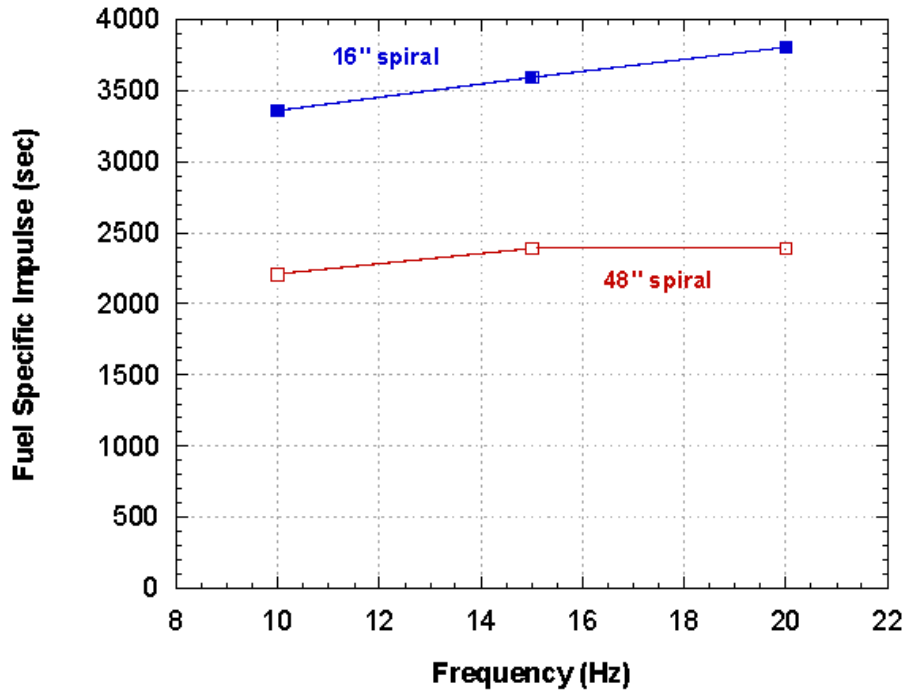
Figure 6. Specific impulse versus frequency for stoichiometric hydrogen-air with 16″ and 48″ spirals in a 72″ long, 2″ diameter tube. Data from [6].

Table 1. Summary of test data from Ref. [6].

| Test Configuration and Data Summary | 2″ tube with 16″ spiral | 3.5″ tube with 16″x 2″ dia spiral | 2″ tube with 1″ dia predet | 3.5″ tube with 1″ dia predet | units |
|---|---|---|---|---|---|
| Total Length | 83 | 91 | 82 | 88 | in |
| Blow-down Time | 3.9 | 5.0 | 5.1 | 4.9 | msec |
| Ignition Time | 1.2 | 0.8 | 1.7 | 2.0 | msec |
| DDT Time | 1.5 | 1.7 | 0.1 | 0.3 | msec |
| Air Thrust | 1 | 2.8 | 1 | 3.8 | lbf |
| Air + Predet Thrust | na | na | 1.6 | 4.8 | lbf |
| Thrust | 6.4 | 25.7 | 9.4 | 30.8 | lbf |
| Integrated Head Pressure | 4.4 | 25.5 | 9.2 | 30.2 | lbf |

12

## III. Detonation Theory

A detonation is a complex event that is unsteady, three-dimensional, and highly sensitive to geometry. Many analytical and theoretical models exist, as well as a large body of experimenatal data describing detonations. The simplest and oldest model of a detonation is Chapman-Jouget (CJ) theory. CJ theory is used to estimate detonation velocities, but provides no insight into the structure of a detonation. The next step up in complexity is the Zeldovich, von Nuemann, and Döring (ZND) model. ZND theory provides details about the structure of a detonation wave, but does not give details about the three-dimensional structure observed in experiments. To understand the three-dimensional structure, smokefoil records, and more recently, CFD simulations are used. The three-dimensional structure has a strong influence on detonation diffraction. Understanding this behavior is critical to developing successful pre-detonators.

### Chapman-Jouget Theory

The simplest model of a detonation is a Chapman-Jouget detonation wave. A CJ wave is based on a one-dimensional, steady analysis that assumes equilibrium conditions on either side of a control volume. The solution requires no knowledge of the actual structure of the detonation wave [2]. An illustration of a CJ detonation wave is shown in Fig. 7. The wave is propagating from left to right in the lab frame of reference. The analysis uses a wave fixed coordinate system that models a standing detonation wave with the reactants moving towards the wave and the products moving away. An analytical solution for the CJ velocity is possible if complete combustion is assumed across the wave. The analytical solution over-predicts measured wave speeds, however. A more accurate solution is given if the detonation products are calculated using equilibrium methods to find the equilibrium concentrations of

13
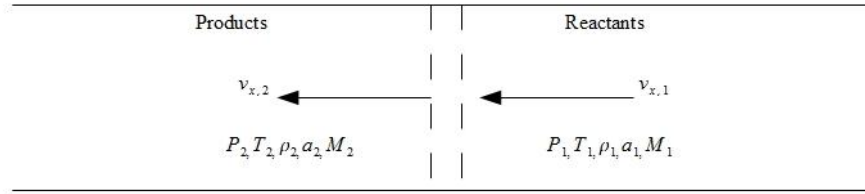
Figure 7. CJ detonation wave propagating from left to right in a wave fixed coordinate system.

reactants, products, and intermediate species. The solution requires an iterative process, but predicts detonation velocities that closely match experimentally measured values.

The basis for CJ theory is the intersection of the Rayleigh line and the Hugoniot curve. The equation for the Rayleigh line can be found by combining the continuity and momentum equations for steady, one-dimensional flow, with no body forces, and no external heat sources [3].

$$\dot{m}^2 = \rho_1^2 u_1^2 = \frac{p_2 - p_1}{\frac{1}{\rho_1} - \frac{1}{\rho_2}} \tag{1}$$

The Hugoniot curve is found by combining the energy equation with the continuity and momentum equations [3].

$$\frac{\gamma}{\gamma - 1}\left(\frac{p_2}{\rho_2} - \frac{p_1}{\rho_1}\right) - \frac{1}{2}(p_2 - p_1)\left(\frac{1}{\rho_1} - \frac{1}{\rho_2}\right) = q \tag{2}$$

The Hugoniot curve shows all possible solutions, $(1/\rho_2, p_2)$, for a given set of initial conditions, $(1/\rho_1, p_1)$, and heat release, $q$. Plotting the Hugoniot curve, there are five regions than can be marked off to show various solutions that are possible, as illustrated in Fig. 8. The point $(1/\rho_1, p_1)$ in the figure is known as the origin of the Hugoniot curve. The curve does not pass through the origin unless the heat release

14
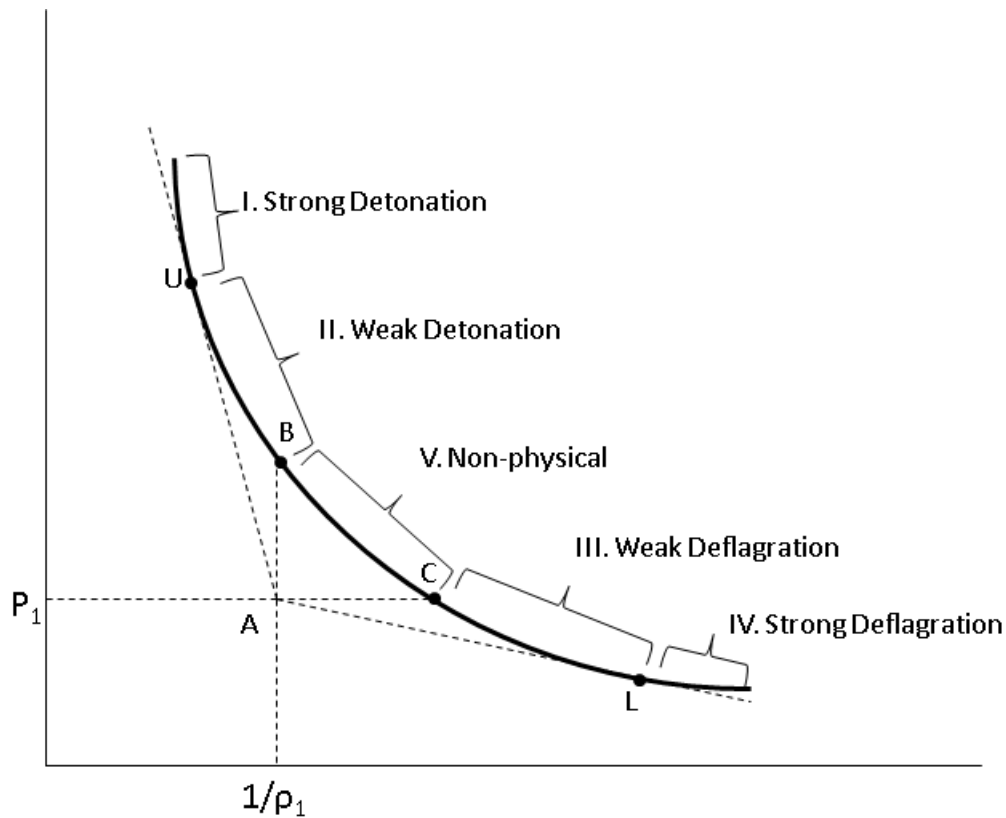
Figure 8. Hugoniot curve showing sections of the curve that correspond to combustion conditions.

is zero. For larger values of the heat release, the Hugoniot curve is further removed from the origin. By drawing the Rayleigh lines through the origin that are tangent to the Hugoniot curve, the upper and lower CJ points can be found (in the figure as points U and L). The upper point represents a detonation and the lower point a deflagration and correspond to a state where the velocity of the wave relative to the burned products is $M = 1$. Additionally, point B represents the intersection with the Rayleigh line for an infinite wave speed and point C represents the intersection with the Rayleigh line for a zero velocity wave. These four points define five regions on the Hugoniot curve. The first region represents a strong detonation, also known as an overdriven detonation, and is defined as a detonation that is propagating faster than the CJ velocity. The second region is a weak detonation and represents a detonation

15

travelling at less than the CJ velocity. The third and fourth regions represent a weak and strong deflagration, respectively. The fifth region represents an area of non-physical solutions since values in this region give an imaginary wave speed in the Rayleigh relation.

Since this research is concerned with detonations, the properties of the upper CJ point will be examined. Strong or overdriven detonations are observed experimentally just after DDT when the detonation is undergoing transient behavior. An overdriven detonation will relax back to the CJ state and this mechanism is explained by CJ theory. At the upper CJ point, the velocity of the wave relative to the burned products is $M = 1$ so disturbances behind the wave cannot affect it. In an overdriven detonation, the velocity of the wave relative to the burned productions is $M < 1$ so any disturbance that creates a rarefaction (expansion) wave can propagate up to the wave and lower its velocity back to the CJ state.

The ultimate goal of this analysis is to provide an estimate of the velocity of a stably propagating detonation wave. An analytical solution for the detonation velocity may be obtained by assuming complete combustion [15].

$$v_D = \left[ 2(\gamma_2 + 1)\gamma_2 R_2 \left( \frac{c_{p,1}}{c_{p,2}} T_1 + \frac{q}{c_{p,2}} \right) \right]^{1/2} \tag{3}$$

The analytical solution over-predicts the actual value of the detonation velocity by not taking into account intermediate species in the products. Due to the high temperature behind the shock, there will be many intermediate species present that will lower the heat release, thereby reducing the CJ velocity. A more accurate method is to use either a trial and error interative method or a Newton-Raphson interation method [3]. Using the Cantera package [16] developed at CalTech, the calculated velocity for a stoichiometric hydrogen/oxygen mixture at 1 atm and 291 K is 2,838 m/s. The experimentally measured value is 2,819 m/s [3].

16

## Zeldovich, von Neumann, and Döring Model

The Zeldovich, von Neumann, and Döring (ZND) model represents a detonation wave as a shock wave follwed by a reaction zone. The thickness of a shock is only a few mean free paths so little or no chemical reactions occur across the shock. Therefore, chemical reactions occur after the shock. Unlike CJ theory, ZND theory provides clues into the structure of a detonation wave. It is still a one-dimensional model and does not explain the three-dimensional structure. ZND theory does give insight into the chemical lengths and induction times of the chemistry. It also predicts a large pressure spike, known as the von Neumann spike, that is observed experimentally.

To obtain a ZND solution, the steady form of the one-dimensional equations for inviscid gas dynamics in a wave fixed frame may be used [16].

$$\frac{d\rho}{dx} = -\frac{\rho}{w}\frac{\dot{\sigma}}{\eta} \tag{4}$$

$$\frac{dw}{dx} = \frac{\dot{\sigma}}{\eta} \tag{5}$$

$$\frac{dP}{dx} = -\rho w \frac{\dot{\sigma}}{\eta} \tag{6}$$

$$w\frac{dY_i}{dx} = \dot{\Omega}_i \tag{7}$$

Note that in the wave fixed frame, $w$, is the velocity. In these equations, $\eta$, is the sonic parameter

$$\eta = 1 - M^2, \tag{8}$$

$\dot{\Omega}_i$ is the rate of change for each species, and $\dot{\sigma}$ is the thermicity. In order to calculate the rate of change for species $i$, a system of algebraic equations representing the chemical reactions that define the system must be solved. The thermicity measures the rate that chemical energy is transformed into thermal energy as well as the reverse process. Changes in thermicity reflect the net effect of all chemical reactions taking

17

place [16]. Thermicity is defined as

$$\dot{\sigma} = \sum_{i=1}^{N_Y} \sigma_i \frac{DY_i}{Dt} \tag{9}$$

where $\sigma_i$ is the thermicity coefficient for chemical species $i$.

A ZND solution using the Cantera package is shown in Fig. 9 for stoichiometric hydrogen/air at standard conditions. Note the von Neumann pressure spike. The



(a) Pressure

(b) Density

(c) Temperature

(d) Species
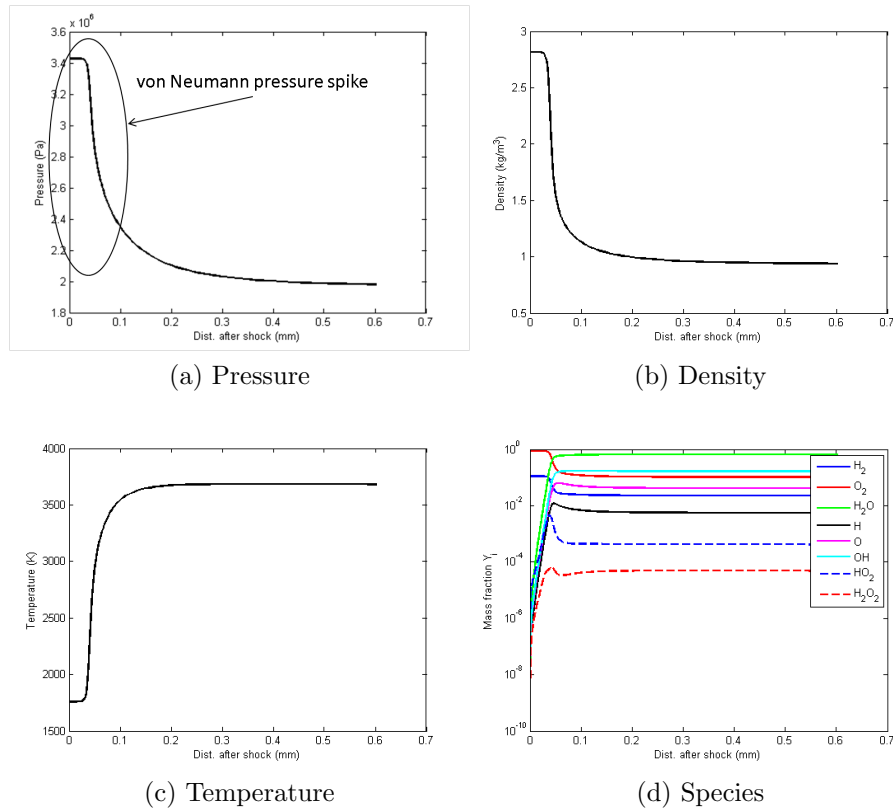
Figure 9. ZND solution for stoichiometric hydrogen/air at standard conditions.

spike is approximately a 30:1 ratio that can be seen in the figure. Note that there is a small distance after the shock where the properties change very slowly, known as the induction zone. After the induction zone, the flow properties change very rapidly as chemical reactions occur. Once the chemical reactions are complete, the solution has reached the equilibrium CJ values for pressure, density, temperature,

18

and species. One important thing to take away from this is the distance in which this occurs. These changes take place is less than a millimeter. Experimentally, in order to resolve these features, a high data sampling rate is necessary due to the high speeds and short distances involved. Compuationally, this means that many nodes or cells are required to resolve the structure of a detonation correctly.

## 3-Dimensional Structure

Smokefoil records show the actual structure of a stably propagating detonation wave is highly three-dimensional. Currently, there is no analytical theory to completely explain this structure. A smokefoil record is made by covering the inside of a pipe with soot and allowing a detonation to propagate down it. On the soot a pattern will be traced that resembles the scales of a fish. The fishscale pattern is a trace of the high pressure transverse waves. Figure 10 shows a numerically generated smokefoil record that is created by taking a peak pressure histogram of the transient data set. Each of the fishscale-like diamonds is known as a detonation cell. The width of this cell, $\lambda$, is dependent upon a variety of factors such as pressure, temperature, and the chemistry of the mixture. The smaller the cell width of the mixture, the easier it is to initiate a detonation. Fuels mixed with pure oxygen have smaller cell widths than those mixed with air, whichis why most pre-detonators require pure oxygen. The smaller cell size means smaller pre-detonators since the critical diameter is smaller.

Figure 11 shows an idealized two-dimensional representation of a smokefoil record. It shows the path of the transverse waves as the detonation progresses. The lines A-I represent various times. Unlike CJ or ZND theory, the velocity of a detonation is constantly changing. Times A, G, and D mark where the transverse waves collide with each other or a wall surface. After this collision, the transverse waves are travelling approximately Mach 8 with respect to the unburnt mixture. When the transverse

www.manaraa.com
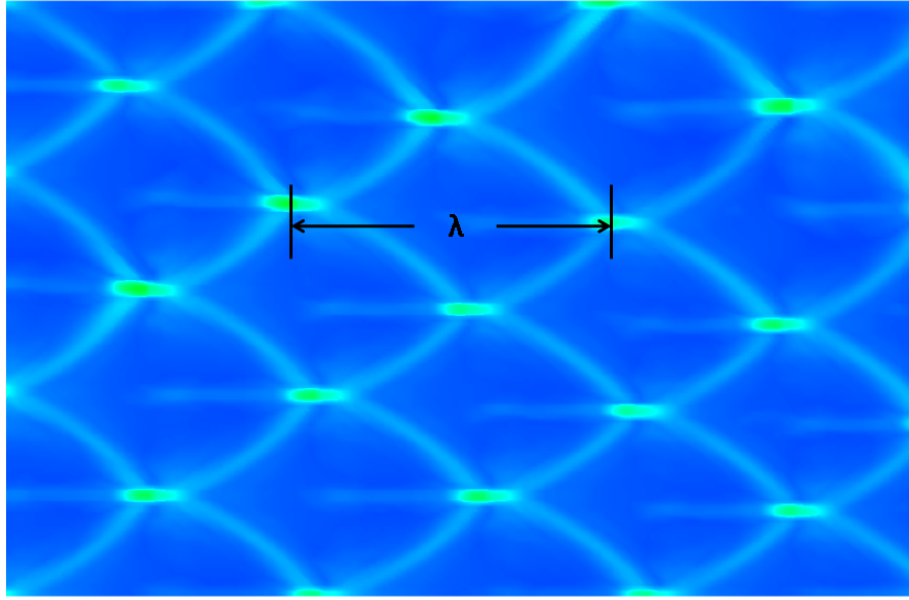
Figure 10. Numerically generated smokefoil record of a detonation.
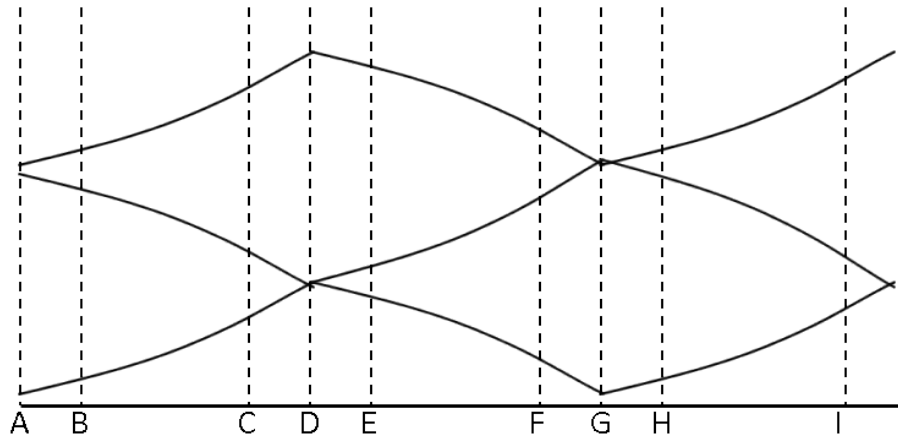


Figure 11. Ideal two-dimensional smokefoil record.

waves reach times C, F, and I, the transverse waves have slowed to approximately Mach 3. The average velocity of these transverse waves is about Mach 5. The reason for this varying velocity has to do with the induction length. After a collision, the induction zone is very small which leads to fast wave speeds. As the wave travels, the induction length increases, thereby slowing the wave down until another collision.

The transverse waves are also known as triple points because they are the inter-

www.manaraa.com

section of three shocks. These three shocks are known as the incident shock, reflected shock, and the Mach stem; and are shown in Fig. 12. To better understand this
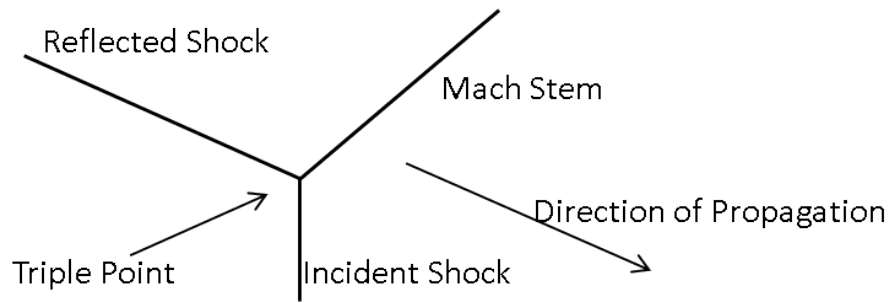


Figure 12. Triple point structure in a propagating detonation wave.

structure, consider a spherical shock wave propagating towards a wall. As the shock hits the wall there is a second shock that is reflected back. The reflected shock merges with the incident shock and creates a Mach stem.

**Detonation Diffraction Physics**

A pre-detonator relies on transitioning a detonation from a smaller area to a larger area. In order for a detonation to propagate into an unconstrained volume, the pre-detonator must be larger than the critical diamter. The critical diameter is 13 cell widths for a circular geometry, 10 for a square, and between 10 and 3 for increasing aspect ratio.

There are three different types of diffraction based on the coupling of the shock and combustion wave during transition. A supercritical transition occurs when the diameter is greater than the critcal diameter. During this diffraction process, the shock and combustion wave stay coupled the entire time as the detonation propagates into the larger area. A critical transition occurs near the critical diameter and is characterized by the temporary decoupling and then recoupling of the shock and combustion front. In a sub-critical transition, the shock wave and combustion wave completely decouple and the detonation becomes a deflagration wave.

21

To numerically model the diffraction process, a two-step or more detailed chemistry model is required. A stably propagating detonation may be modeled by a one-step global reaction model, but the transient diffraction process requires a more realistic model. The requirement is necessary to correctly capture critical and subcritical transitions. A one-step global model does not take into account the induction time for the chemical reactions so there is no distance between the shock and the start of the chemical reactions. Therefore, the one-step model does not accurately capture the decoupling process that can occur. A two-step or more detailed model does take into account the induction delay and can match experimental Schlieren images of detonation diffractions.

## IV. DETON-2D

The research conducted in this thesis uses a code known as DETON-2D developed by Dr. Viswanath Katta [8, 17]. It is a finite difference code that solves the two-dimensional Euler equations with the two-step global chemistry model of Korobeinikov [18] on a Cartesian grid. The solver utilizes a 2nd-order MacCormack predictor-corrector technique [19] with a 4th order flux corrected transport (FCT) scheme for damping and anti-diffusion [20, 21]. Wall boundary conditions are set as reflective slip walls. DETON-2D is capable of accurately resolving the transverse wave structure, CJ wave speed, and the detonation diffraction physics that are observed experimentally.

### Governing Equations

The governing equations for DETON-2D are the two-dimensional Euler equations. The chemistry is represented by a two-step, global chemistry model. The chemistry tracks two progress variables to model an induction period followed by a heat release and is known as the Korobeinikov model [18]. The full set of equations, in conservation form, are given as

$$\frac{\partial Q}{\partial t} + \frac{\partial E}{\partial x} + \frac{\partial F}{\partial y} + H = 0 \tag{10}$$

where

$$Q = \begin{bmatrix} \rho \\ \rho u \\ \rho v \\ E \\ \rho \beta \\ \rho \alpha \end{bmatrix}, \ E = \begin{bmatrix} \rho u \\ \rho u^2 + p \\ \rho u v \\ u(E+p) \\ \rho \beta u \\ \rho \alpha u \end{bmatrix}, \ F = \begin{bmatrix} \rho v \\ \rho u v \\ \rho v^2 + p \\ v(E+p) \\ \rho \beta v \\ \rho \alpha v \end{bmatrix}, \ H = \begin{bmatrix} 0 \\ 0 \\ 0 \\ 0 \\ c\rho \dot{w}_\beta \\ c\rho \dot{w}_\alpha \end{bmatrix}. \tag{11}$$

23

In $H$, $c$ is the inverse freestream speed of sound and $\dot{w}_\alpha$ and $\dot{w}_\beta$ are the rates of change for the progress variables $\alpha$ and $\beta$. The progress variables track the progress of the chemical reactions occuring in the flow and are explained in more detail in the next section.

**Korobeinikov Model**

The Korobeinikov model is a global reaction model. Chemical processes are generalized to consist of two steps. The first step is an irreversible induction reaction and models the delay between the heating of the reactants and the start of the chemical reactions. The second step is an exothermic heat release and models the energy given off by the chemical reactions taking place in flow. The variables $\alpha$ and $\beta$ are known as progress variables and track the progress of both of these steps. In the source term $H$ in Eqn. 11, the rates of change of the progress variables, $\dot{w}_\beta$ and $\dot{w}_\alpha$, are given by

$$\dot{w}_\alpha = \frac{\partial \alpha}{\partial t} = -\frac{1}{\tau_{ind}} = -k_1 \rho \exp(-E_1/RT) \tag{12}$$

$$\dot{w}_\beta = \frac{\partial \beta}{\partial t} = -k_2 p^2 [\beta^2 \exp(-E_2/RT) - (1-\beta)^2 \exp(-(E_2+q)/RT)]. \tag{13}$$

Note that these equations are similar in form to the Arrhenius equation. The constants $k_1$ and $k_2$ are pre-exponential factors and $E_1$ and $E_2$ are activation energies. The value, $q$, is the heat release of the reaction. Both $\alpha$ and $\beta$ are set to 1 initially. The first reaction is $\dot{w}_\alpha$ and $\alpha$ progresses from 1 to 0 while $\beta=1$ to model the induction reaction. Once $\alpha=0$, $\dot{w}_\beta$ progresses and $\beta$ goes from 1 to 0 to model the exothermic reaction. The effect the heat release in the flow is modeled in the equation of state given by

$$p = (\gamma - 1)[E - \rho\beta q - 0.5\rho(u^2 + v^2)]. \tag{14}$$

24

Equations 12 and 13 require the temperature in dimensional form. This is given by the ideal gas law as

$$T = \frac{a_\infty p}{\rho R} \tag{15}$$

where $a_\infty$ is introduced due to the non-dimensionalization of $p$ and $\rho$. The parameters for the chemistry model are chosen to represent stoichiometric hydrogen/oxygen with 70% argon dilution.

Table 2. Parameters in Korobeinikov chemistry model for $H_2/O_2/Ar$.

| | |
|---|---|
| $k_1$ | $18.75 \times 10^6$ |
| $k_2$ | $4.5941 \times 10^3$ |
| $E_1/R$ | 9800 |
| $E_2/R$ | 2000 |
| $Q$ | $4.0 \times 10^10$ |
| $\gamma$ | 1.4 |

**Cartesian Grid Methods**

DETON-2D solves the governing equations on a Cartesian grid. A Cartesian grid is a grid where the distribution of nodes in the $x$ and $y$ directions are parallel to the Cartesian axes. An ideal Cartesian grid in that every node is equidistant and $\Delta x = \Delta y$ as shown in Fig. 13. This type of grid provides the highest accuracy possible
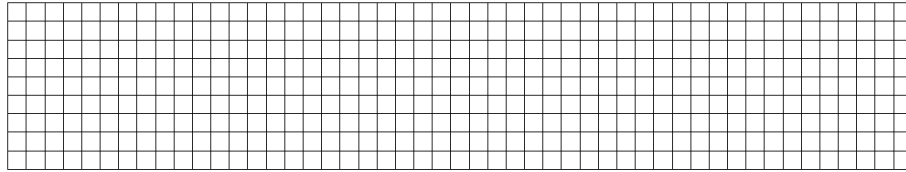


Figure 13. Ideal Cartesian grid.

of the discretized formulas [22]. An additional benefit is that no grid transformations are necessary. However, this only allows for orthogonal geometries so curves and angled surfaces cannot be easily represented. Geometry in the flow is represented

by disregarding nodes that are within the boundaries of the solid object as shown in Fig. 14. Representing the geometry in this fashion simplifies the problem since only a single computational block is required to represent the entire domain. The
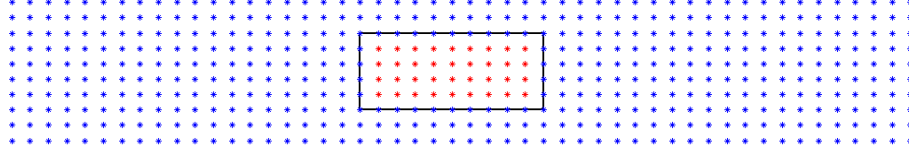


Figure 14. Cartesian grid with geometry. Blue represents nodes in the domain and red nodes are disregarded.

grid spacing is based on the ZND induction length for the chemistry. The induction length, $L^*$, is 0.2933 cm and is unique to the mixture. A spacing of $\frac{2}{9}L^*$ is used. The detonation cell width is about $9L^*$ which corresponds to approximately 40 nodes per detonation cell. Previous work has shown that this resolution accurately captures cellular structure, CJ wave speed, and diffraction phenomena [8, 17].

**Numerical Solver**

The numerical method used to solve the governing equations is MacCormack's method with a 4th order flux corrected transport scheme for damping and anti-diffusion. MacCormack's method provides second order accuracy in space and time and the FCT scheme provides an accurate representation of shocks in the flow. Mac-Cormack's method is a predictor-corrector technique developed in 1969 [19]. Flux corrected transport was introduced in 1973 [20]. The solver may be thought of as comprising of four steps. The first step is the predictor step of MacCormack's method, the second step is the corrector step of MacCormack's method, the third step is to add fourth order damping terms, and the fourth and final step is to apply the FCT scheme. The scheme is similar to the MacCormack-FCT scheme [21], with the exception of the additional fourth order damping terms.

The first part of the numerical solver is to progress the solution one time step into the future using MacCormack's method. The method itself is comprised of two steps, the predictor step and the corrector step. The predictor step uses a forward difference to calculate the derivative at a point.

$$\left(\frac{\partial Q}{\partial t}\right)_{i,j}^{t} = -\left(\frac{E_{i+1,j}^{t} - E_{i,j}^{t}}{\Delta x} + \frac{F_{i,j+1}^{t} - F_{i,j}^{t}}{\Delta y} + H_{i,j}^{t}\right) \tag{16}$$

The predicted values at time $t + \Delta t$ are then found by progessing the solution one step in time with Euler's method as follows.

$$(\bar{Q})_{i,j}^{t+\Delta t} = Q_{i,j}^{t} + \left(\frac{\partial Q}{\partial t}\right)_{i,j}^{t} \Delta t \tag{17}$$

The corrector step uses the predicted values at time $t + \Delta t$ to find the derivative at time $t + \Delta t$ using a backward difference.

$$\left(\frac{\overline{\partial Q}}{\partial t}\right)_{i,j}^{t+\Delta t} = -\left(\frac{(\bar{E})_{i,j}^{t+\Delta t} - (\bar{E})_{i-1,j}^{t+\Delta t}}{\Delta x} + \frac{(\bar{F})_{i,j}^{t+\Delta t} - (\bar{F})_{i,j-1}^{t+\Delta t}}{\Delta y} + (\bar{H})_{i,j}^{t+\Delta t}\right) \tag{18}$$

The derivative at that point is now calculated as the average of the two derivatives.

$$\left(\frac{\partial Q}{\partial t}\right)_{av} = \frac{1}{2}\left[\left(\frac{\partial Q}{\partial t}\right)_{i,j}^{t} + \left(\frac{\overline{\partial Q}}{\partial t}\right)_{i,j}^{t+\Delta t}\right] \tag{19}$$

Now the corrected and final values are given by

$$Q_{i,j}^{t+\Delta t} = Q_{i,j}^{t} + \left(\frac{\partial Q}{\partial t}\right)_{av} \Delta t. \tag{20}$$

The actual expressions used in the code are very similar, however they are more compact to save on memory requirements for running the code. The first step is

27

given by

$$Q_{i,j}^{(1)} = Q_{i,j}^n - \frac{\Delta t}{\Delta x}[E_{i+1,j}^n - E_{i,j}^n] - \frac{\Delta t}{\Delta y}[F_{i,j+1}^n - F_{i,j}^n] - \Delta t H_{i,j}^n \qquad (21)$$

and the second step by

$$Q_{i,j}^{(2)} = \frac{1}{2}\left[Q_{i,j}^n + Q_{i,j}^{(1)} - \frac{\Delta t}{\Delta x}[E_{i,j}^{(1)} - E_{i-1,j}^{(1)}] - \frac{\Delta t}{\Delta y}[F_{i,j}^{(1)} - F_{i,j-1}^{(1)}] - \Delta t H_{i,j}^{(1)}\right]. \qquad (22)$$

Before the FCT step is done, the third step is to add fourth-order damping for stability and to damp out oscillations given by

$$
\begin{aligned}
Q_{i,j}^{(3)} =&\, Q_{i,j}^{(2)} - d_x[E_{i+2,j}^n - 4E_{i+1,j}^n + 6E_{i,j}^n - 4E_{i-1,j}^n + E_{i-2,j}^n]\\
&- d_y[F_{i,j+2}^n - 4F_{i,j+1}^n + 6F_{i,j}^n - 4F_{i,j-1}^n + F_{i,j-2}^n]
\end{aligned}
\qquad (23)
$$

where $d_x$ and $d_y$ are the damping coefficients.

The fourth step is the flux corrected transport step consisting of a diffusion and anti-diffusion step. The diffusion step is given by

$$Q_{i,j}^{(4)} = Q_{i,j}^{(3)} + \eta_x(Q_{i+1,j}^n - 2Q_{i,j}^n + Q_{i-1,j}^n) + \eta_y(Q_{i,j+1}^n - 2Q_{i,j}^n + Q_{i,j-1}^n) \qquad (24)$$

where $\eta_x$ and $\eta_y$ are diffusion coefficients. The equation adds artificial viscosity to the solution in order to damp out oscillations and maintain positivity. However, the diffusion tends to smooth out discontinuities in the flow. Therefore, an anti-diffusion step is done given by

$$Q_{i,j}^{n+1} = Q_{i,j}^{(4)} - (\delta_{i+1/2} - \delta_{i-1/2}) - (\delta_{j+1/2} - \delta_{j-1/2}). \qquad (25)$$

The anti-diffusion step removes the diffusion from the previous step while limiting

28

the solution so that no new extrema are produced. By limiting the solution, the anti-diffusion step maintains second-order accuracy except in regions of strong discontinuites, where the solution becomes first-order. The limiting process is known as flux correction and is accomplished in the $\delta$ terms given by

$$\delta_{i+1/2} = S \max[0, \min(S\Delta^{(4)}_{i-1/2}, \eta|\Delta^{(3)}_{i+1/2}|, S\Delta^{(4)}_{i+3/2})] \tag{26}$$

where

$$\Delta_{i-1/2} = Q_{i,j} - Q_{i-1,j} \tag{27}$$

$$\Delta_{i+1/2} = Q_{i+1,j} - Q_{i,j} \tag{28}$$

$$\Delta_{i+3/2} = Q_{i+2,j} - Q_{i+1,j} \tag{29}$$

$$\Delta_{j-1/2} = Q_{i,j} - Q_{i,j-1} \tag{30}$$

$$\Delta_{j+1/2} = Q_{i,j+1} - Q_{i,j} \tag{31}$$

$$\Delta_{j+3/2} = Q_{i,j+2} - Q_{i,j+1} \tag{32}$$

and $\Delta^{(3)}$ uses $Q^{(3)}$ and $\Delta^{(4)}$ uses $Q^{(4)}$. The values of $S$ are given by

$$S = \text{sign}(\Delta^{(3)}_{i+1/2}) \tag{33}$$

or

$$S = \text{sign}(\Delta^{(3)}_{j+1/2}). \tag{34}$$

For the $\delta$ terms with $j$ indicies, the previous equations are the same with the $i$ indices being replaced by the $j$ indices.

## V. Pre-detonator Geometries

Simple geometries are tested to determine how a detonation diffracts from a pre-detonator to a thrust tube. The two main geometries tested are a symmetric step expansion and a corner reflector. Parametric studies are conducted on the two geometries. Additionally, it is found that the success of transition from pre-detonator to thrust tube depended on more than just the geometry. The transverse wave structure of the detonation at the transition affects success. In an experiment, the part of the transverse wave structure at the transition is random. Therefore, the part of the transverse wave structure at the transition is varied to estimate the success rate by varying the length of the pre-detonator.

The data at the end of the simulation shows whether or not a detonation transitioned. Post processing is done in Tecplot. The three sets of data used to determine if a detonation is occuring are the smokefoil record, instantaneous pressure, and instantaneous temperature. Figure 21 shows a successful detonation transition. The top is the pressure histogram followed by the pressure and then temperature. Note the cellular stucture of the pressure histogram (smokefoil record). Also, note that both the pressure and temperature are coupled. Figure 22 shows a detonation that has become a deflagration wave after the abrupt expansion. Note that the pressure and temperature are no longer coupled.

**Symmetric Step Expansion**

The symmetric step expansion is the simplest concept. An initial parametric study is done to determine the success rates of a pre-detonator with an initial height, expanding into a thrust tube of a given expansion ratio. Flat plate obstructions are then introduced into the thrust tube near the exit of the pre-detonator. Parametric studies are done varying the height of the flat plate and the distance from the abrupt

30

expansion. The base cases without any flat plate are given in Table 3 where $E$ is the expansion ratio, $E = L/l$. Additional parametric studies are done on each

Table 3. Base cases for pre-detonator heights.

| $l$ $(\lambda)$ | $E$ | | | | | | | | | |
|---|---|---|---|---|---|---|---|---|---|---|
| 1 | 1.5 | 2 | 2.5 | 3 | - | - | - | - | - | - |
| 1.5 | 1.5 | 2 | 2.5 | 3 | - | - | - | - | - | - |
| 2 | 1.5 | 2 | 2.5 | 3 | 3.5 | 4 | 4.5 | 5 | 5.5 | 6 |
| 2.5 | 1.5 | 2 | 2.5 | 3 | 3.5 | 4 | 4.5 | 5 | 5.5 | 6 |

pre-detonator and expansion ratio combination to determine the effect a flat plate obstruction has on detonation transition. The parameters studied are given Fig. 15. The height, $h$, and distance, $d$, of the flat plates are varied to find regions of high success.
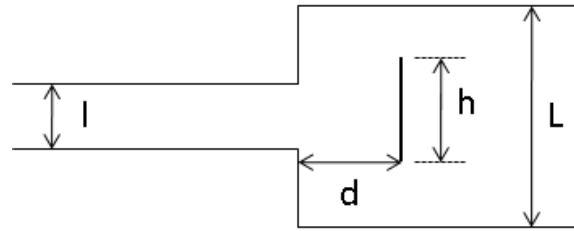


Figure 15. Parameters for symmetric step expansion cases.

## Corner Reflection Geometries

A corner reflection geometry attempts to take advantage of a strong 180 degree reflection off a wall; however, a detonation reflecting 180 degrees off of a wall reflects back into products. Since a detonation requires an unburnt fuel-oxidizer mixture in order to propagate, a detonation that reflects back into itself will die out. The pre-detonators being studied are below the critical diameter, so the decoupling of the shock and combustion wave allows for the possibility that the shock reflects into the unburnt mixture. The parameters are shown in Fig. 16. The expansion rato and

31

distance are varied for pre-detonator hieghts of 0.5 and 1 $\lambda$ to find regions with high success rates.
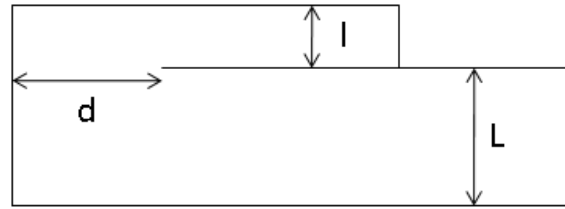


Figure 16. Parameters for corner reflection cases.

**Success Rates**

The geometries being studied are all less than the critical diameter of 3 cell widths for a two-dimensional detonation. In a lab setting, a 2d detonation experiment is done with a high aspect ratio, rectangular pre-detonator. Comparison of these results to 2d numerical simulations show that the simulations capture and predict the correct physics [10]. Experimental results [5] have also shown success rates in detonation transitions. The success rate is believed to be due to the transverse wave structure of a detonation. The transverse wave structure repeats itself periodically in space as it progresses down a tube as shown in Fig. 17. Experimentally, the phase of this
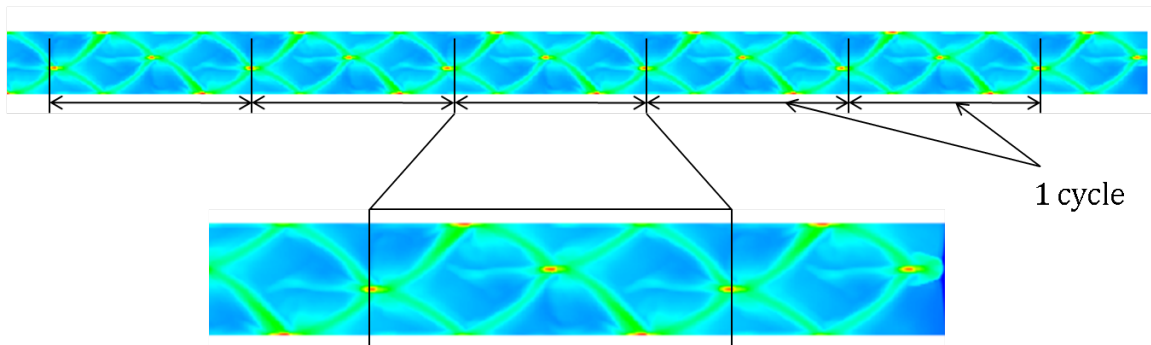


Figure 17. Repeating transverse wave structure in a stably propagating detonation wave.

periodic structure is random. To determine this success rate numerically, the location

32

of the abrupt expansion (pre-detonator exit) is changed with respect to the transverse wave over one cycle. The methodology assumes that the probability of any part of the transverse wave structure occuring at the abrupt expansion is uniformly distributed.

To ensure that the probabilities of success and failure repeat itself each cycle, simulations were conducted where the pre-detonator lenght was varied over a distance of 10 $\lambda$. Figure 18 shows the distribution of successes and failures for a pre-detonator with $l = 1.5 \lambda$ and $E = 1.5$. A repeatable pattern emerges in the success and failure
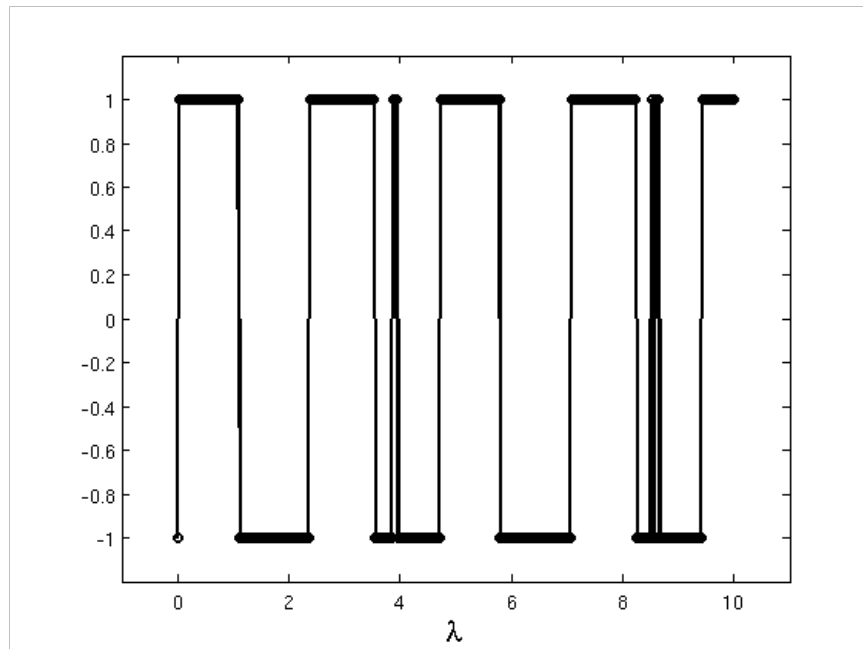


Figure 18. Distribution of successes and failures for $l = 1.5 \lambda$, $E = 1.5$ by varying pre-detonator length over 10 $\lambda$ (successes are 1, failures are -1).

rates. Marking where the pattern begins and ends shows that the pattern occurs over the cycles of the transverse wave structure as seen in Fig. 19. The success rate over 1 cycle is approximately 50%. Success or failure is dependent upon the strength of reflection off of the thrust tube walls. Successful cases had strong reflections, whereas failures had weaker reflections. A successful wall reflection is shown in Fig. 20a. An unsuccessful reflection is shown in Fig. 20b.

For all parametric studies done, the pre-detonator length was varied by 5 com-
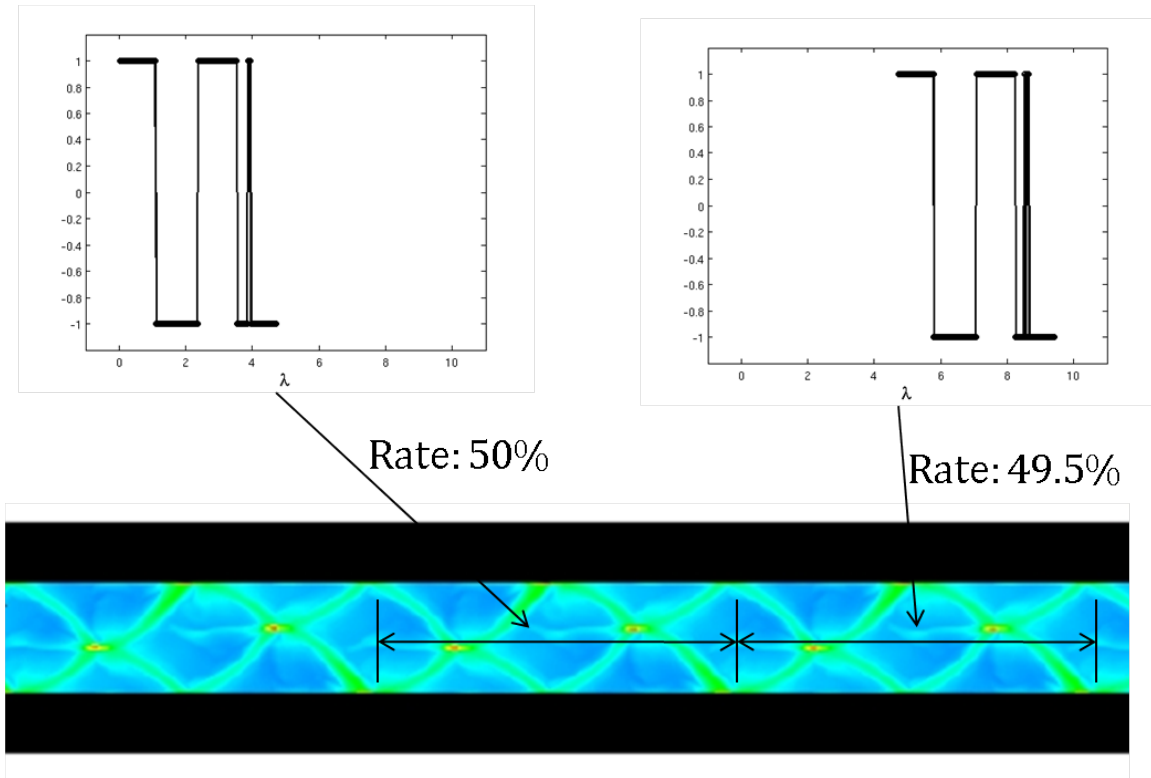
Figure 19. Repeating pattern of successes and failures occuring over transverse wave structure cycles.



(a) Success                    (b) Failure
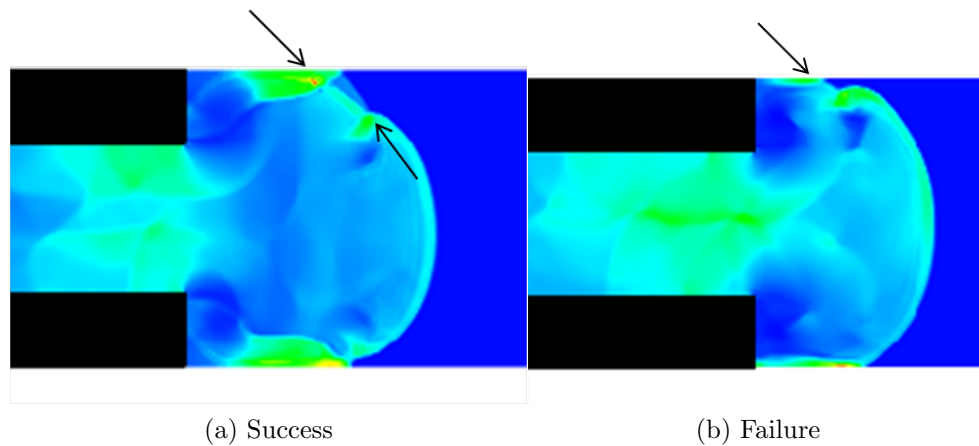
Figure 20. Successful and unsuccessful transitions due to thrust tube wall reflections.

putational nodes for each simulation. The length was varied over 1 cycle of the transverse wave structure for the given pre-detonator height. The success rate is the number of successes divided by the total number of simulations. Success or failure

34

was determined by examining the results at the end of each simulation to determine if the shock and combustion front were still coupled.

## VI. Results and Discussion

Experimental results claim that the critical diameter for a two-dimensional channel is 3 cell widths. The cases being run are focused on subcritical diameter geometries. Since the diameters are subcritical, the success or failure of a transition is dependent upon the transverse wave structure at the exit of the pre-detonator. Geometrical configurations are examined to determine which ones have high success rates. Cases with high success rates are further examined in order to understand the reasons they are successful while others are not. Once the mechanisms behind successful transitions are found, they can be used a basis in recommending future pre-detonator concepts and designs.

### Symmetric Step Expansion Results

The first set of cases for the symmetric step expansion geometries had no flat plate obstructions to determine the effectiveness of adding them later. The success rates are given in Table 4. The success rates are also plotted as a contour map in Fig. 23. For a pre-detonator with a height of 1 $\lambda$, the success rate is 34% into a thrust tube that is 1.5 times larger. Increases in the expansion ratio decrease this rate to zero. The same behavior is seen with a pre-detonator of height 1.5$\lambda$. The success rate for an expansion ratio of 1.5 is 74% and then proceeds to decrease for increasing expansion ratio. The pre-detonator of height 2$\lambda$ shows different qualitative behavior than the smaller pre-detonators. For an expansion ratio of 1.5, the 2 $\lambda$ pre-detonator has a 100% success rate. This success rate decreases and then increases again to 83% at an expansion ratio of 3. The success rate then stays constant and finally decreases for expansion ratios larger than 5. The pre-detonator of height 2.5$\lambda$ shows the same type of behavior. Behavior where a larger expansion ratio has a higher success rate than a smaller expansion ratio has been observed experimentally. In

36

Ref. [5], an expansion ratio of 1.97 had a higher success rate than an expansion of 1.53 for ethylene/air detonations across a step expansion. One explanation [5] is that the larger geometry may produce reflections that are more likely to release sufficient energy for re-initiation. The CFD results show the effect is actually due to the increased separation of the shock and combustion front during the diffraction. Figure 25 shows an unsuccessful transition with $l = 2 \lambda$ and $E = 2$, whereas Fig. 26 shows a successful transition with $E = 3$ for the same pre-detonator height. Both geometries have a strong shock reflection off of the bottom wall. However, the separation of the shock and combustion front is greater for the $E = 3$ case. After the reflection, a detonation wave travels along the compressed yet unreacted region between the shock and combustion front. The slightly larger separation for the $E = 3$ case allows for a larger detonation wave that can survive all the way to the top wall. This wave then reflects off the wall and further downstream generates new triple points until a stably propagating detonation wave is formed.

The effect of adding an obstruction to the flow varies depending on the height and distance of the obstruction. Sometimes the success rate is increased, decreased, or unaffected. Examining the physics that occur in obstructions that increase the success rate may lead to practical pre-detonators. For pre-detonators with a height of $1\lambda$, the success rates are given in Tables 6, 5, and 7 for expansion ratios of 1.5, 2, and 2.5, respectively. The corresponding contour maps are given Figs. 24, 27, and 28. For an expansion ratio of 1.5, an obstruction with $h = 0.5 \lambda$ and $d = 3 \lambda$ increases the success rate from 34% to 96%. Trends in the data suggest that a small plate placed farther out from the expansion is the most successful for transitioning a detonation from the pre-detonator to the thrust tube.

There are two different types of transitions that appear to be occuring for these cases. The first is that the obstruction appears small enough to allow a detonation

37

wave to go past it when the detonation had already successfully transitioned before the obstacle. Fig. 29 shows that the shock wave and combustion wave are coupled before the obstacle and the smokefoil record shows that the detonation wave successfully propagated around the obstacle. The second case is that the obstruction acts similar to a DDT device after the shock and combustion wave have decoupled. The obstruction allows for shock reflections to cause the mixture to auto-ignite resulting in a detonation wave. Figure 30 illustrates the reignition of the detonation wave off of the obstacle. Detonation failure did occur in a small number of cases and appears to be caused by an unsuccessful re-ignition by waves reflected off of the obstruction as shown in Fig. 31. Similar results are obtained for the 1 $\lambda$ pre-detonator for expansion ratios of 2 and 2.5. With an expansion ratio of 2, a flat plate with $d = 3.5\lambda$ and $h = 0.75\lambda$, increases the success rate to 100%. Likewise, a flat plate with $d = 4.5$ $\lambda$ and $h = 1.25$ $\lambda$ corresponds to the highest success rate (60%) for the $E = 2.5$ case. It appears that for increasing expansion ratios, increasing the distance and height of a flat plate obstruction gives the highest success rates.

Pre-detonators with a height of 1.5 $\lambda$ show similar trends to the 1 $\lambda$ case. Results are presented in Tables 8, 9, 10, and 11. Contour maps of the success rates are given in Figs. 32, 33, 34, and 35. For the $E = 1.5$ case, an obstruction with $h = 0.25$ $\lambda$ and $d = 3.5$ $\lambda$ gives a success rate >90%. For larger expansion ratios, the highest success rates occur for increasing values of $h$. Unlike the $l = 1$ $\lambda$ case, the distance decreases to 2.5 $\lambda$ and stays constant for the highest success rates for increasing expansion ratio. The mechanisms behind the success rates are the same as those found for the $l = 1$ $\lambda$ pre-detonators which are reignition upstream, reignition from the obstacle, and failure.

Increasing the pre-detonator height to 2 $\lambda$, an additional triple point is present in the detonation structure. Results are presented in Tables 12, 13, 14, and 15. Contour

38

maps of the success rates are given in Figs. 36, 37, 38, 39. Unlike the $l = 1$ and 1.5 $\lambda$ pre-detonator heights, the optimal flat plate for $l = 2$ $\lambda$ is on the order of the height of the pre-detonator and only 1 $\lambda$ away with the exception of the $E = 1.5$ case. Figure 40 shows results from the $l = 2$ $\lambda$, $E = 4$, $h = 3$ $\lambda$, and $d = 1$ $\lambda$ case where the success rate is 100%. The obstacle reflects the shockwaves so that they reflect off of the back, top, and bottom walls of the thrust tube. Some of these reflections generate detonation waves. Also, the shockwaves from the top and bottom meet in the middle of the thrust tube after the obstable, which initiates a detonation in a manner similar to an implosion.

### Corner Reflection Results

The corner reflector is a simple geometry that attempts to utilize a strong reflection off of a surface to transition a detonation from a pre-detonator to a thrust tube. The parameters studied are the distance to the wall and the expansion ratio for a given pre-detonator height. The success rates for a pre-detonator with a height of 0.5 $\lambda$ is given in Table 16 with the corresponding contour map in Fig. 41. According to the results, there are two areas where a detonation successfully transitions, separated by a region where they do not. The lower left section has lower success rates than the upper right section. The highest success rates (over 90 %) occured for expansion ratios of 3.5 and 4 when the wall was 2 $\lambda$ from the exit of the pre-detonator. The most successful cases occur due to two shock waves converging at a corner; causing an explosion to occur that initiated the detonation in the thrust tube and may be seen in Fig. 43.

Results for $l = 1$ $\lambda$ are given in Table 17 and Fig. 42. Unlike the $l = 0.5$ $\lambda$ case, the $l = 1$ $\lambda$ case appears to only have one region where detonations are successful. A 100% success rate is obtained for an expansion ratio of 3 and a distance of 3 $\lambda$. The

transition mechanism is similar to the $0.5\lambda$ case.

# VII. Conclusions

Numerical simulations of detoantion waves can be used to design pre-detonators. However, multiple simulations are necessary in order to obtain correct results. One-time simulations of a geometrical configuration produce misleading results. Multiple simulations are more compuationally expensive, but provide probabilities of success that are found experimentally. The probabilities of success are a result of the transverse wave structure of a detonation. Success or failure is dependent upon where the pre-detonator exit occurs relative to the transverse wave structure.

The CFD results also provide insight into the physical mechanisms behind successful versus unsuccessful transitions. Common mechanisms for transitioning a detonation into a thrust tube were observed among all cases with high success rates. Wall reflections were the most important mechanism in allowing a detonation to survive transition. Additionally, separation between the shock front and combustion front during diffraction plays an important role in certain cases. In some successful configurations, shock-shock collisions were able to reignite the detonation wave. Any new pre-detonator configurations should attempt to make use of these mechanisms in order to ensure they work 100% of the time.

Parametric studies were conducted on two geometrical configurations to find designs with high success rates. For the symmetric step expansion case, it was found that introducing a flat plate obstruction into the flow can increase the success rate if placed correctly. Corner reflectors were able to transition a detonation at larger expansion ratios than the symmetric step configurations. For both configurations, contour maps of the success rates show peaks that correspond to high probabilities of success. Pre-detonators should be designed so that they fall on those peaks in order to ensure they work at or near 100% efficiency.

41

**Future Work**

The results of the numerical simulations need experimental verification to test the hypothesis that the transverse wave structure is the main contributing factor to the probabilistic nature of detonation diffraction. Computational results have matched trends observed with experimental ethylene/air detonations but a comparison with the hydrogen, oxygen, and argon chemistry of DETON-2D is required.

New geometries should be tested that try to take advantage of the mechanisms that made the studied geometries successful. Corners where shock waves converge can be used to generate explosions to ensure a detonation survives an expansion. Additionally, regions where the shock front and combustion front have decoupled can be used to create an overdriven detonation. Geometries representative of crossover tubes in branched detonation setups should be tested using the method presented to determine their effectiveness.

# Figures
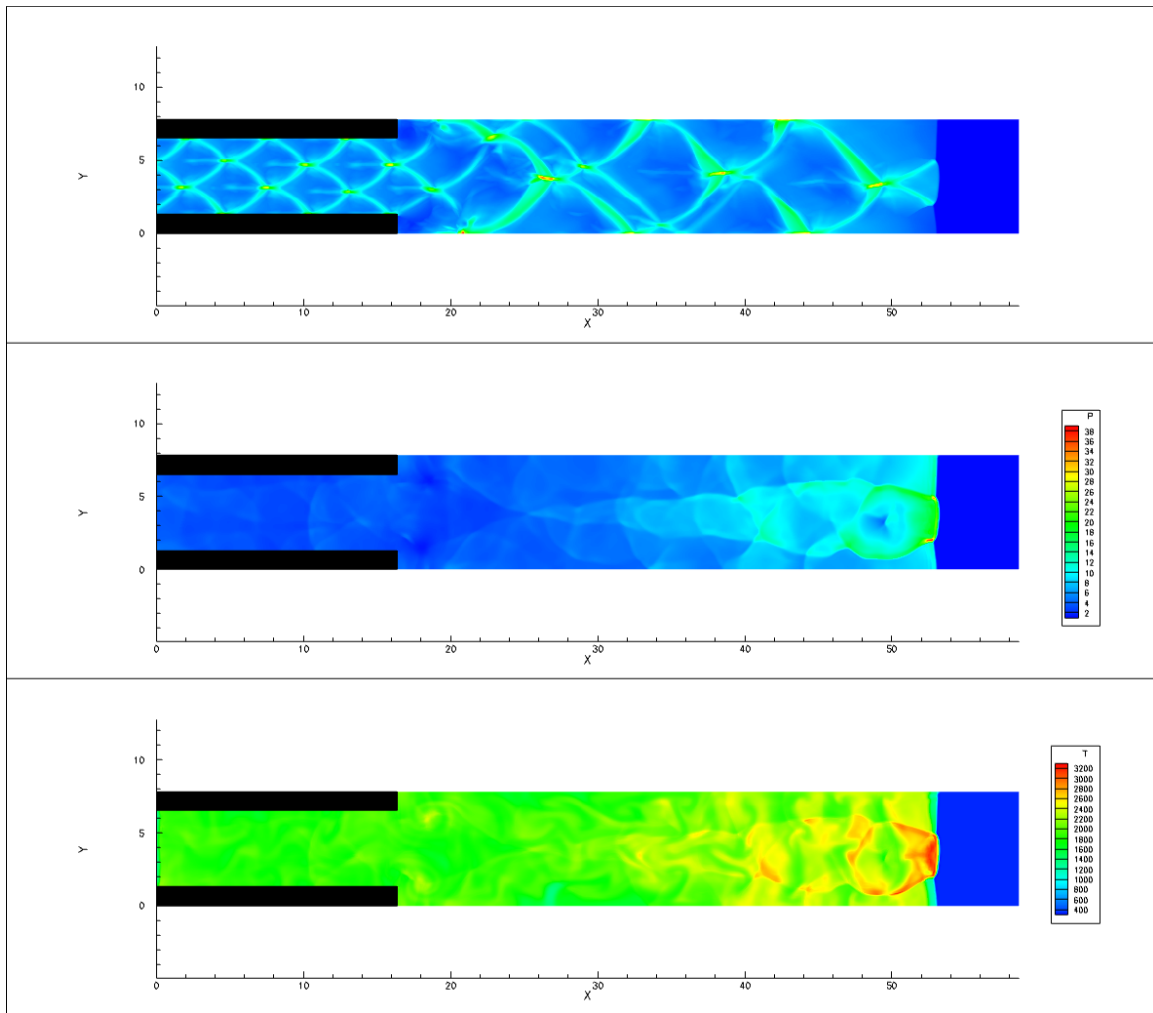


Figure 21. Successful transition of detonation for $l = 2\ \lambda$, $E = 1.5$.
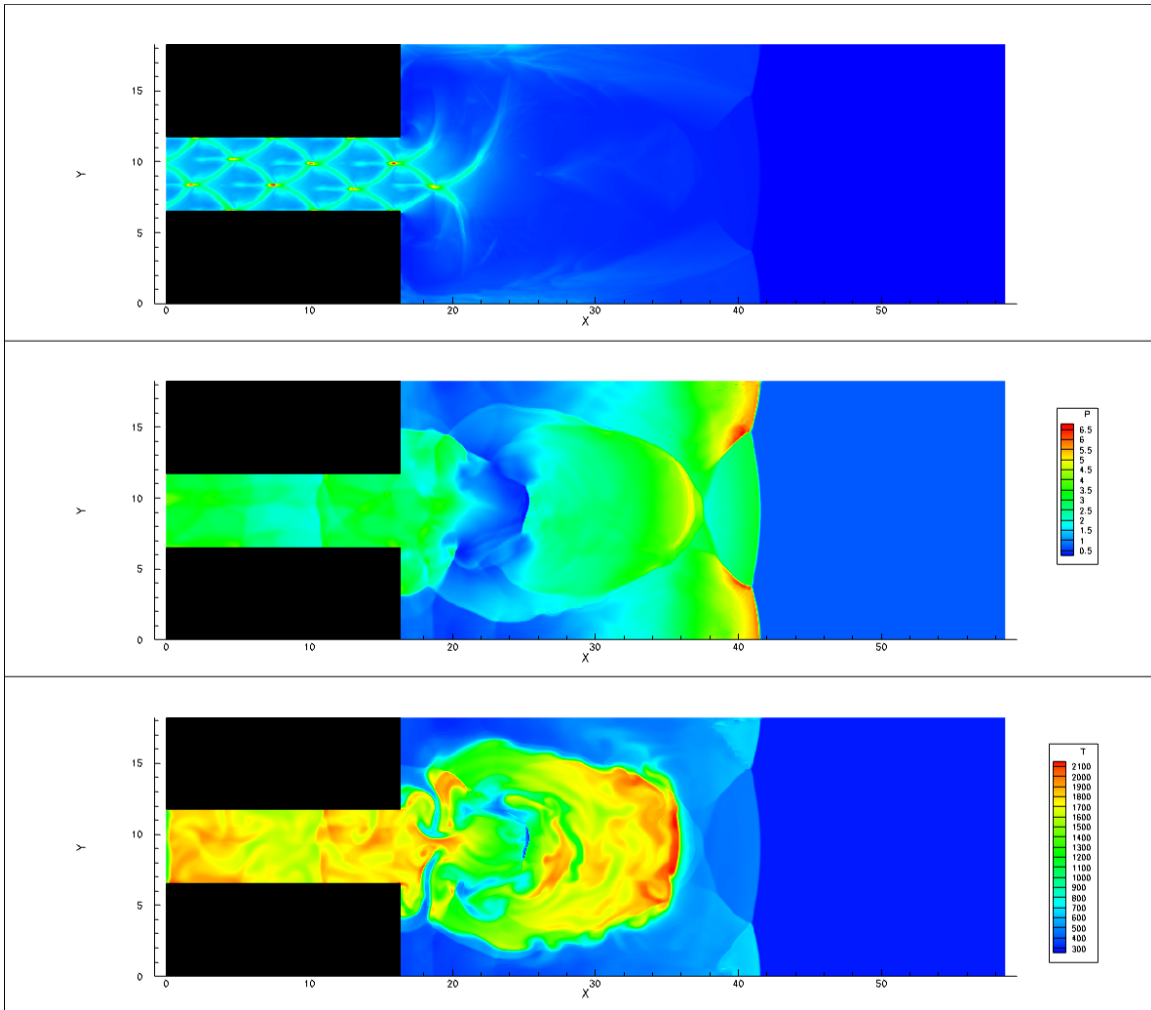
Figure 22. Unsuccessful transition of detonation for $l = 2\ \lambda$, $E = 3.5$.
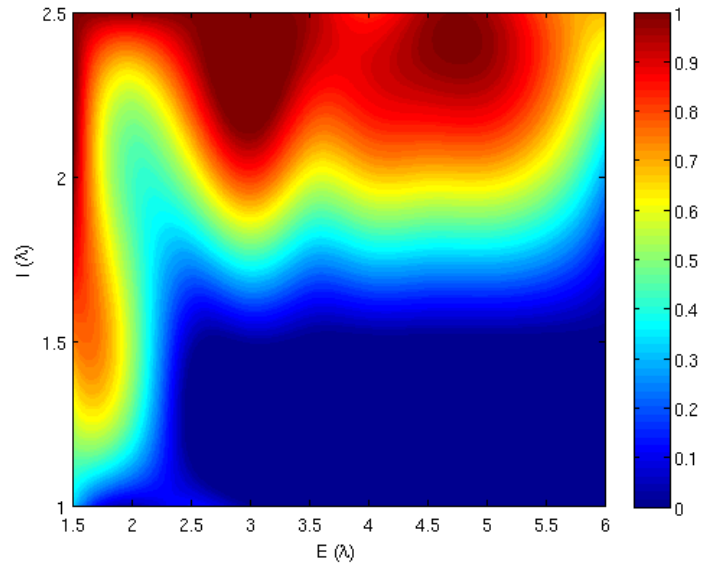
Figure 23. Contour map of success rates for symmetric step expansion base cases (no obstruction).



Figure 24. Contour map of success rates for symmetric step expansion with flat plate ($l = 1$ $\lambda$, $E = 1.5$).

45
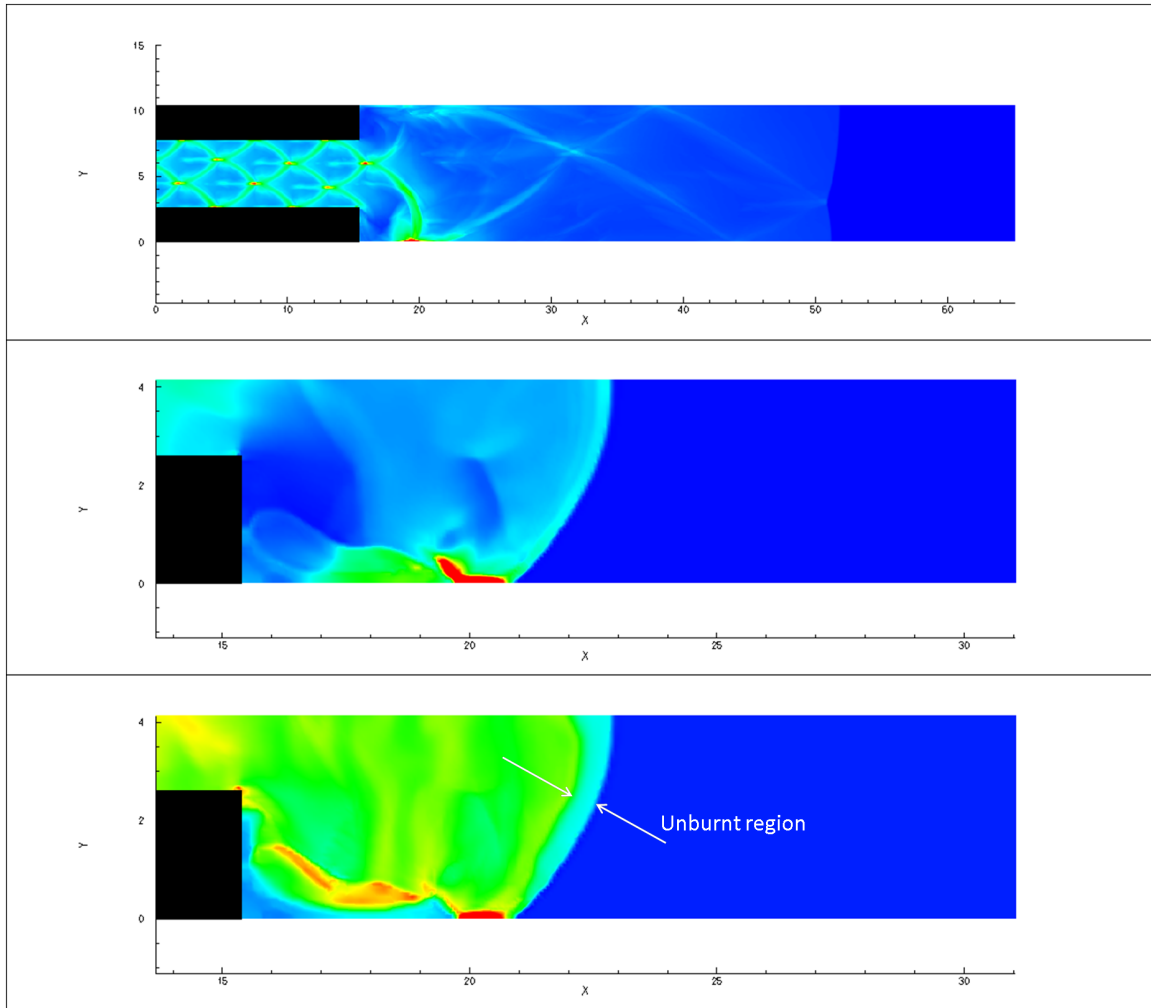
Figure 25. Unsuccessful transition with $l = 2\ \lambda$ and $E = 2$.

Figure 26. Successful transition with $l = 2 \lambda$ and $E = 3$.
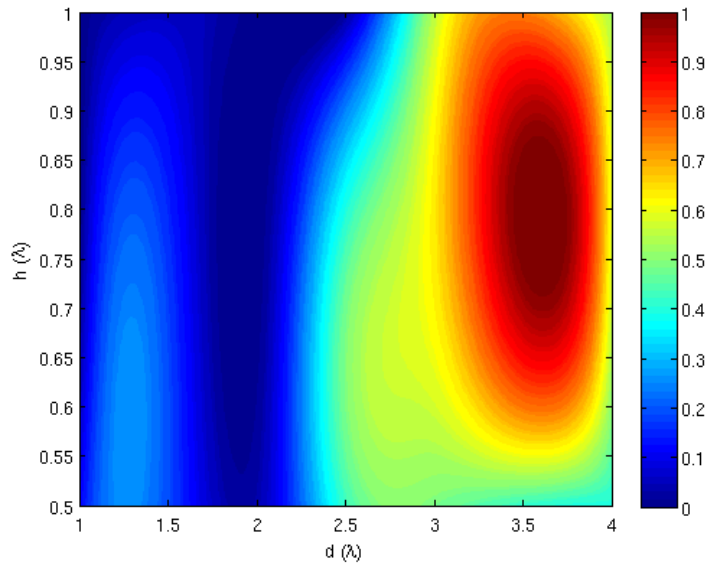
Figure 27. Contour map of success rates for symmetric step expansion with flat plate ($l = 1\ \lambda$, $E = 2$).
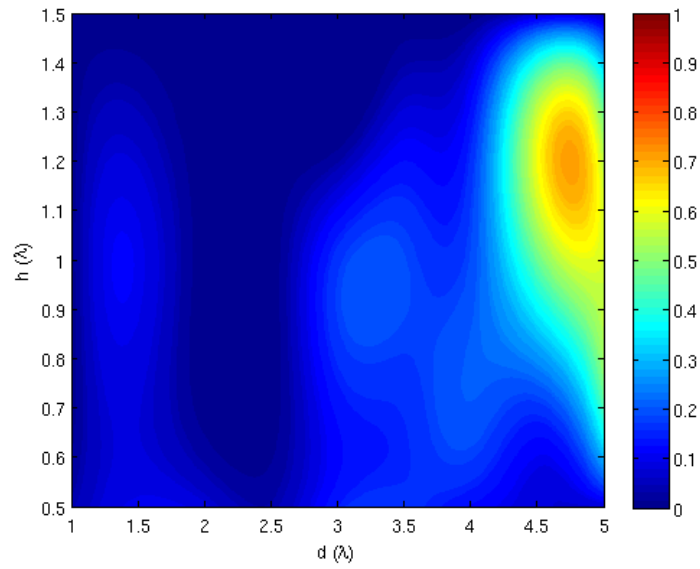


Figure 28. Contour map of success rates for symmetric step expansion with flat plate ($l = 1\ \lambda$, $E = 2.5$).

48
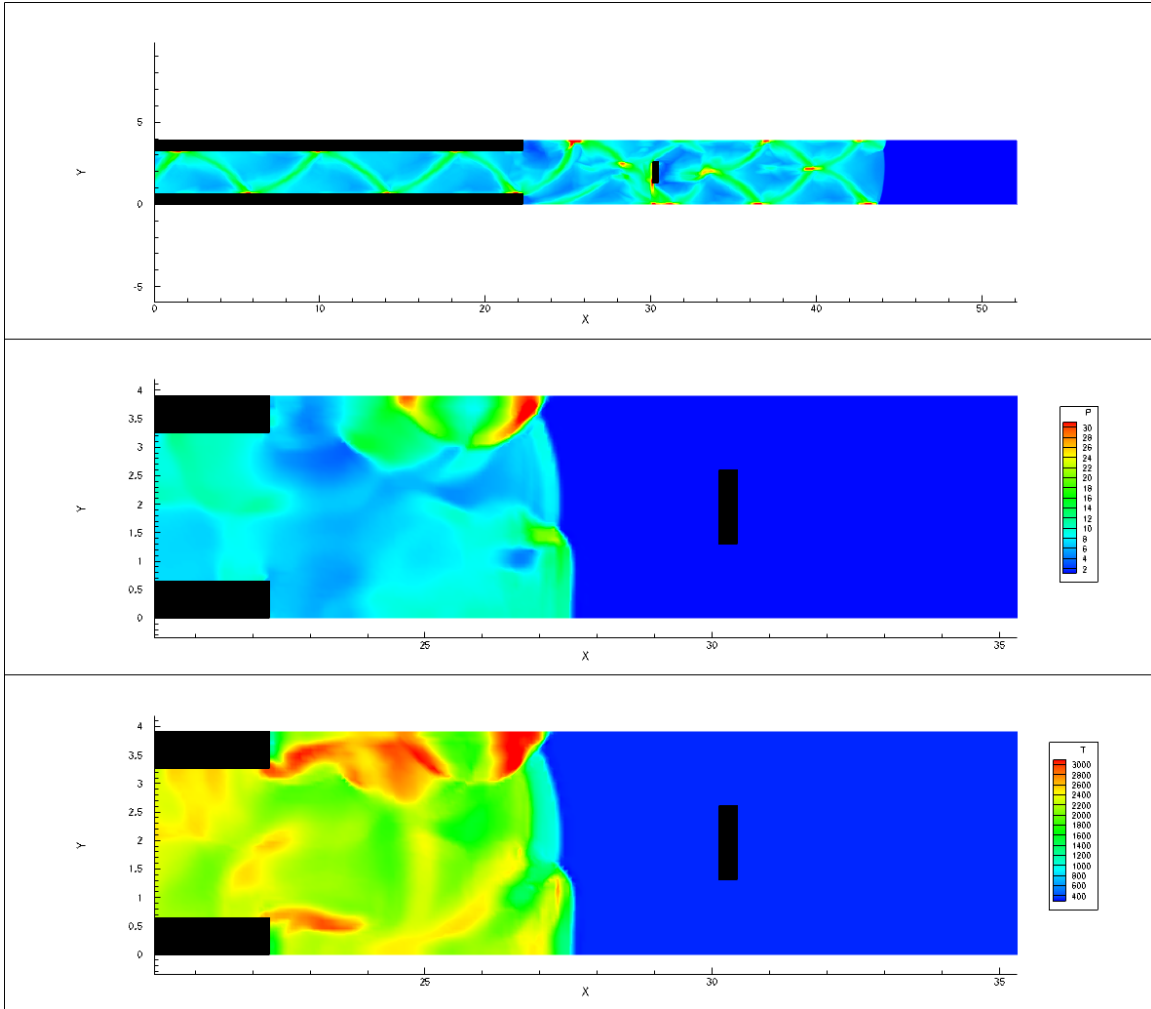
Figure 29. Successful transition for $l = 1$ $\lambda$, $E = 1.5$, $h = 0.5$ $\lambda$, and $d = 3$ $\lambda$ with ignition upstream of the obstacle.
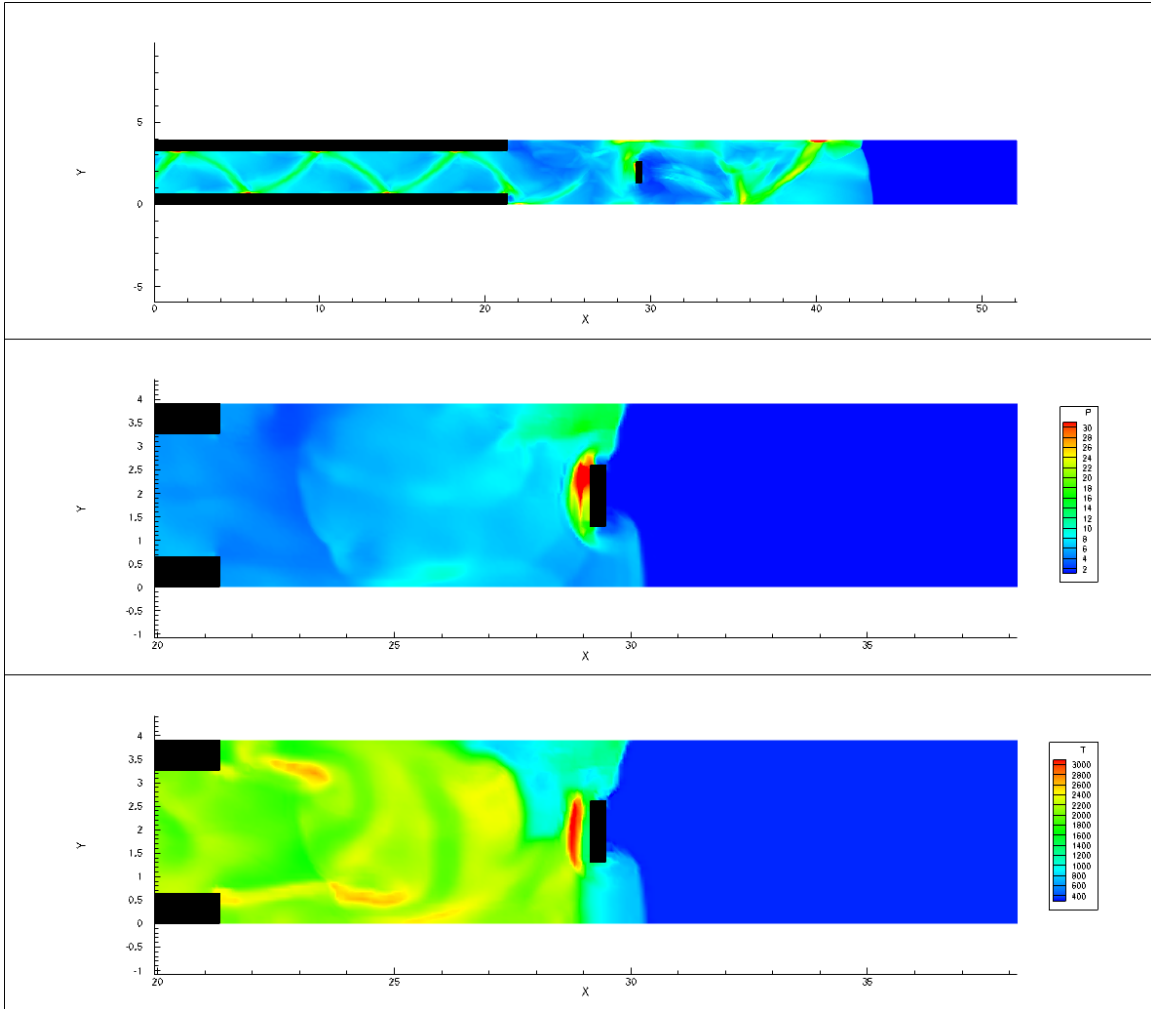
Figure 30. Successful transition for $l = 1\lambda$, $E = 1.5$, $h = 0.5\lambda$, and $d = 3\lambda$ with ignition due to obstacle.
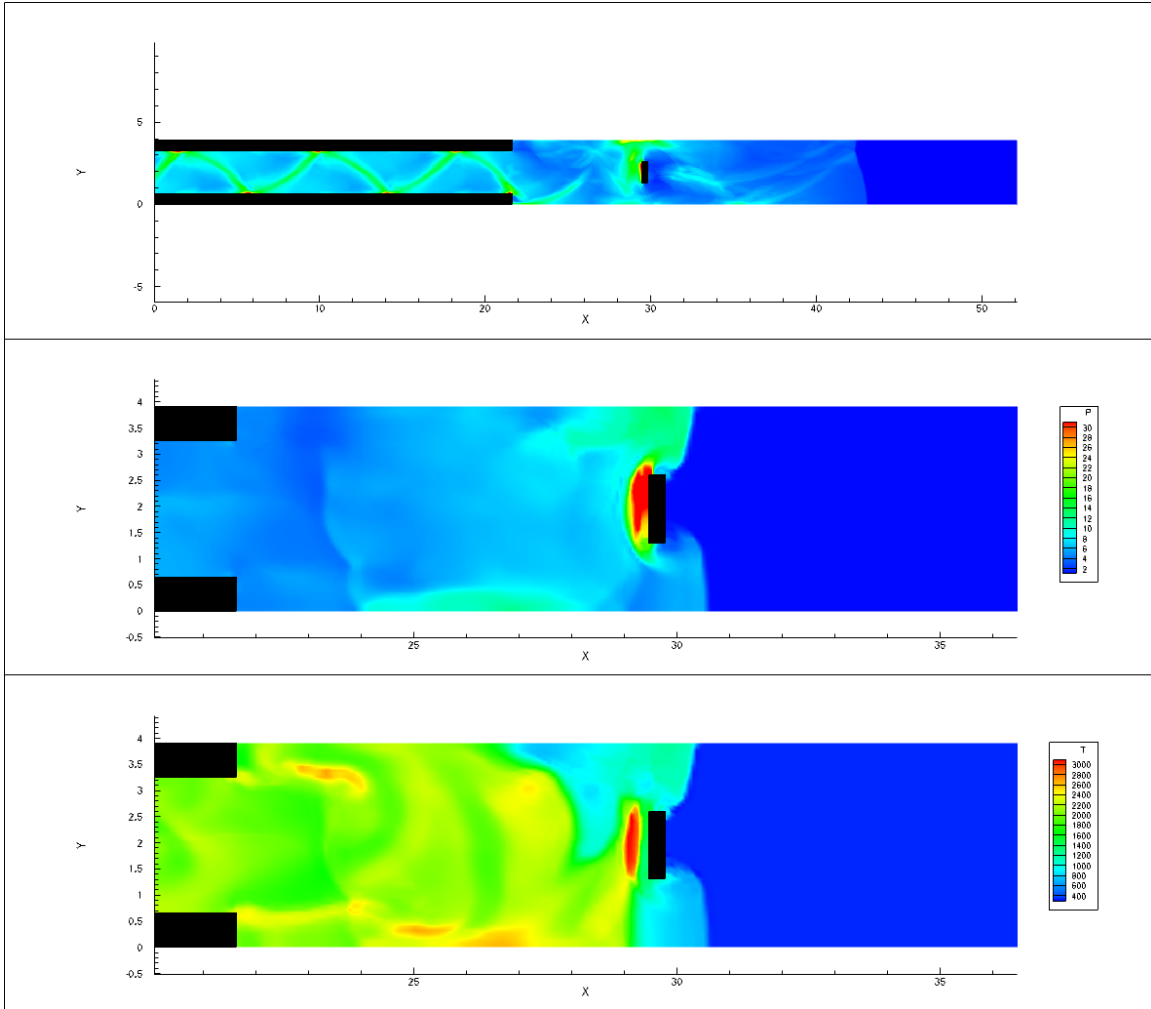
Figure 31. Unsuccessful transition for $l = 1$ $\lambda$, $E = 1.5$, $h = 0.5$ $\lambda$, and $d = 3$ $\lambda$ with obstacle failing to reignite detonation.
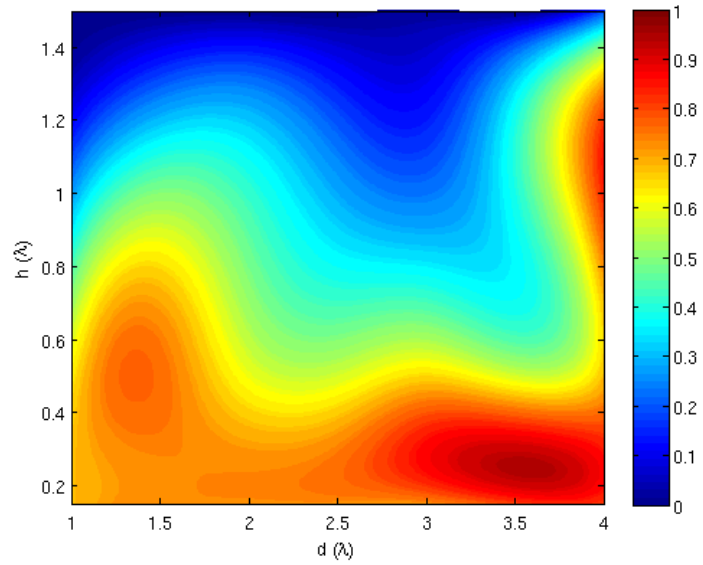
Figure 32. Contour map of success rates for symmetric step expansion with flat plate
($l = 1.5\ \lambda$, $E = 1.5$).
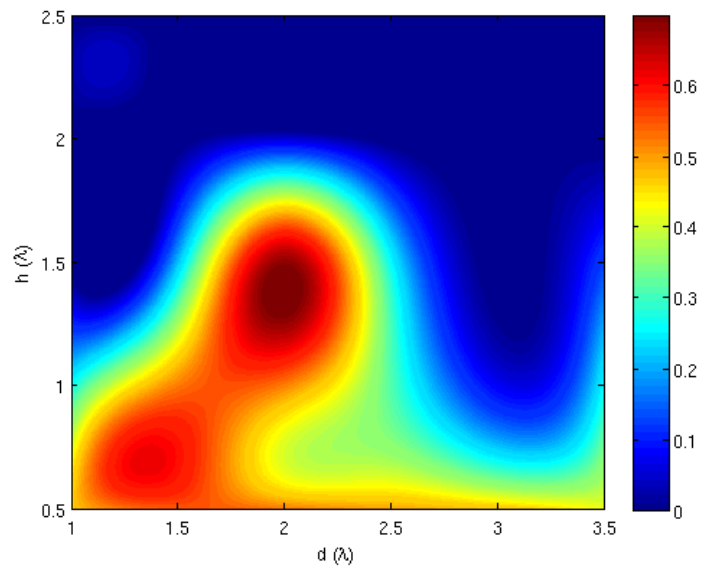


Figure 33. Contour map of success rates for symmetric step expansion with flat plate
($l = 1.5\ \lambda$, $E = 2$).
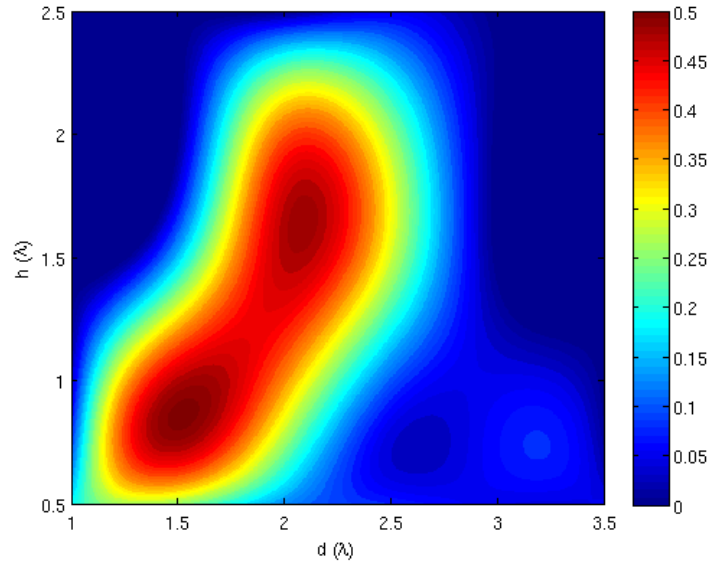
Figure 34. Contour map of success rates for symmetric step expansion with flat plate ($l = 1.5\ \lambda$, $E = 2.5$).
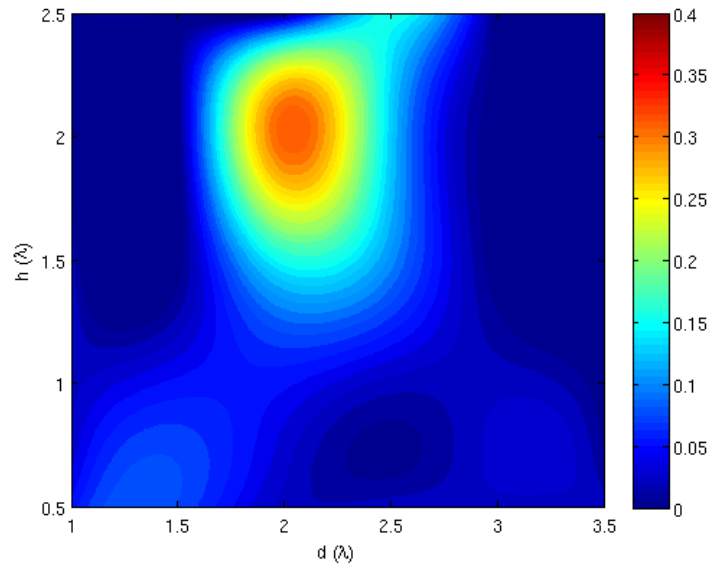


Figure 35. Contour map of success rates for symmetric step expansion with flat plate ($l = 1.5\ \lambda$, $E = 3$).

53
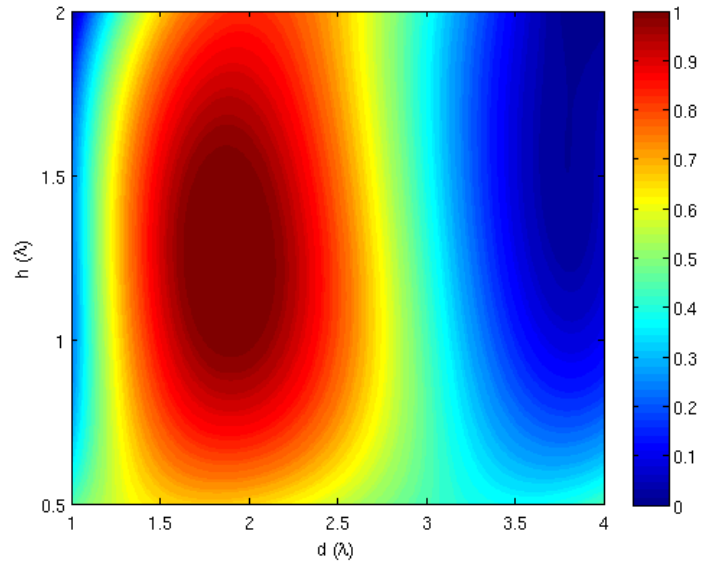
Figure 36. Contour map of success rates for symmetric step expansion with flat plate ($l = 2\ \lambda$, $E = 2$).
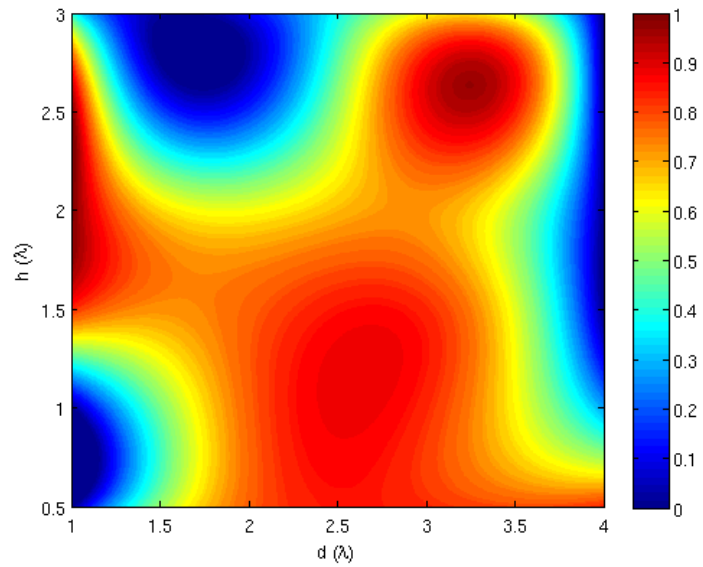


Figure 37. Contour map of success rates for symmetric step expansion with flat plate ($l = 2\ \lambda$, $E = 3$).

54
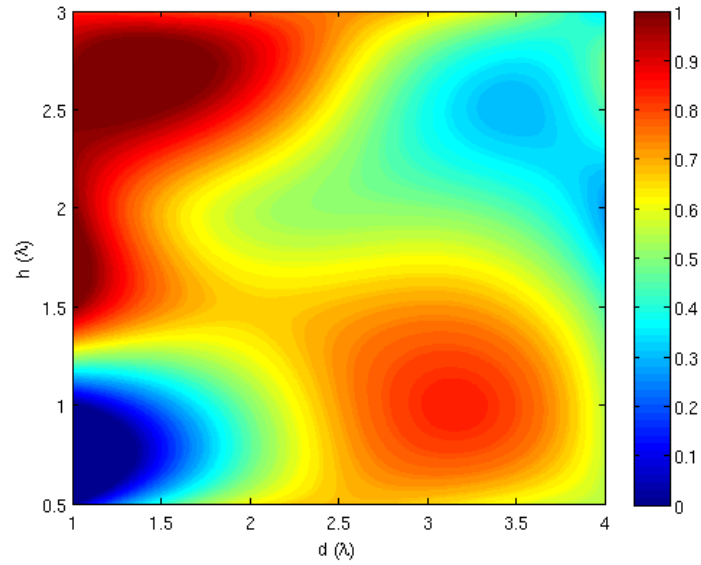
Figure 38. Contour map of success rates for symmetric step expansion with flat plate $(l = 2 \lambda, E = 4)$.
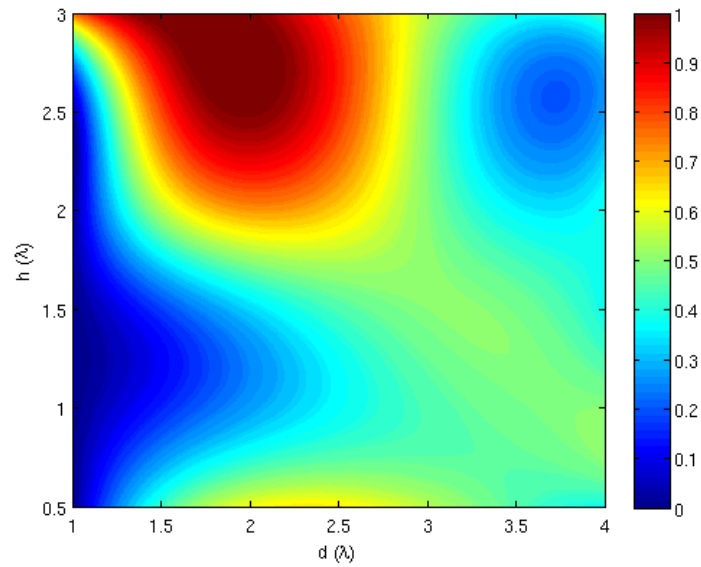


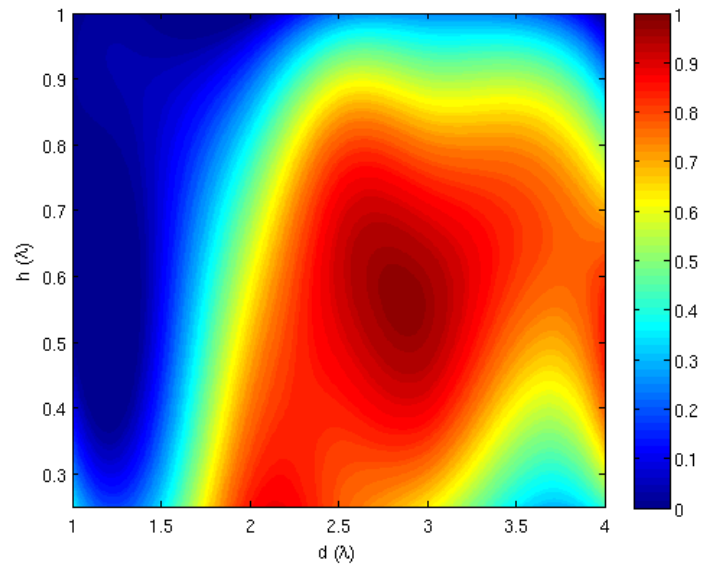Figure 39. Contour map of success rates for symmetric step expansion with flat plate $(l = 2 \lambda, E = 5)$.
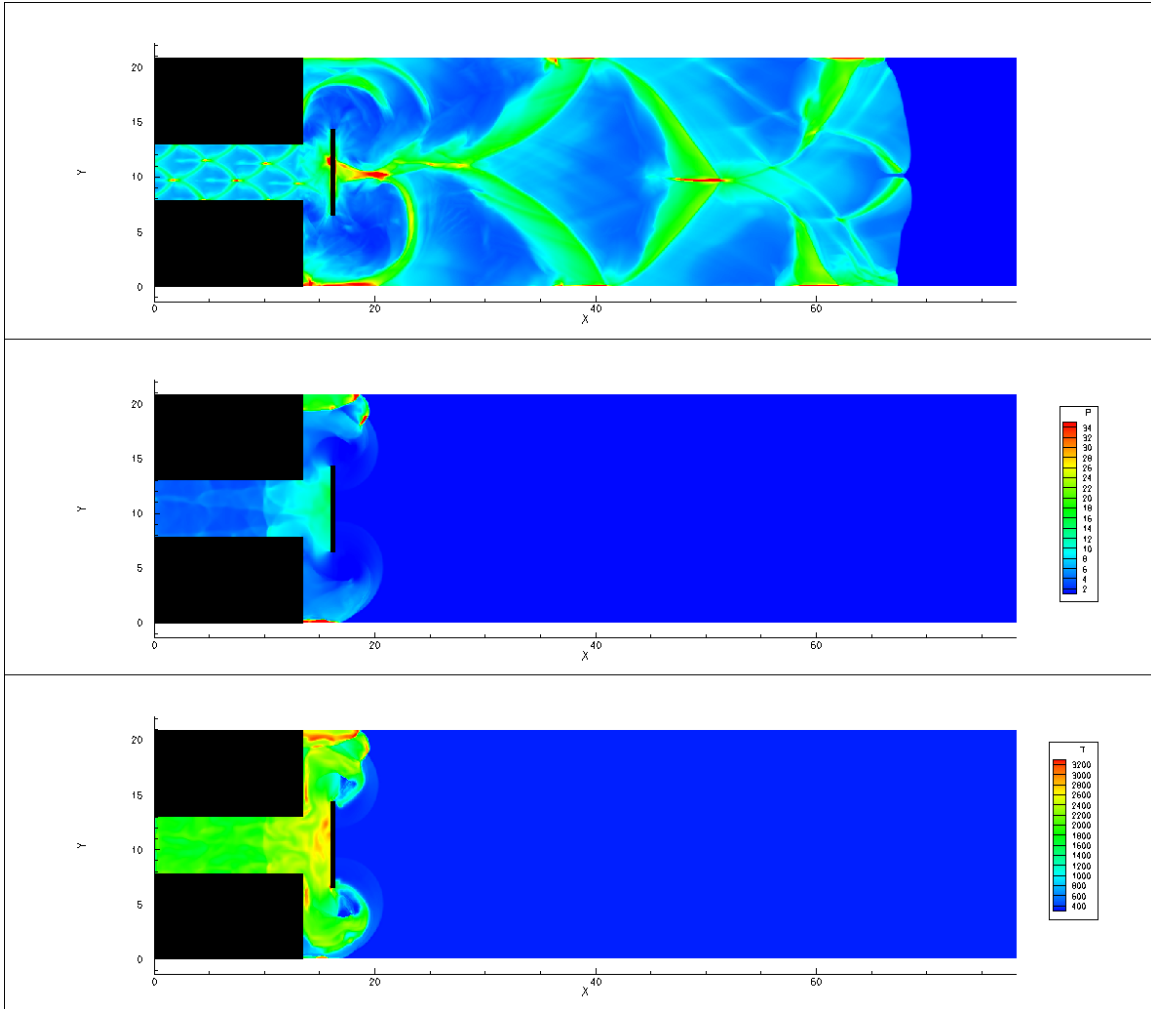
Figure 40. Successful transition for $l = 2\lambda$, $E = 4$, $h = 3\lambda$, and $d = 1\lambda$ with ignition due to strong wall reflections.
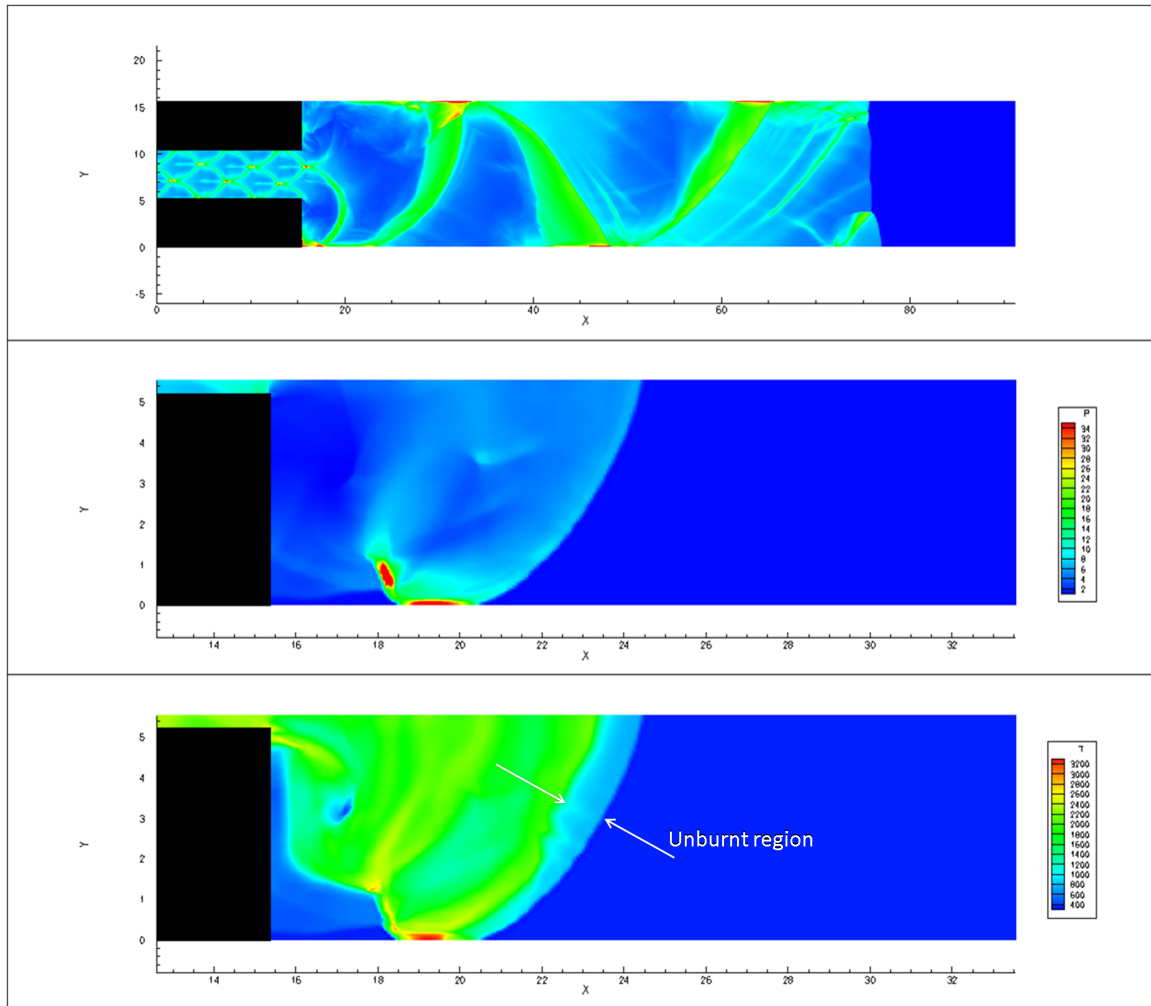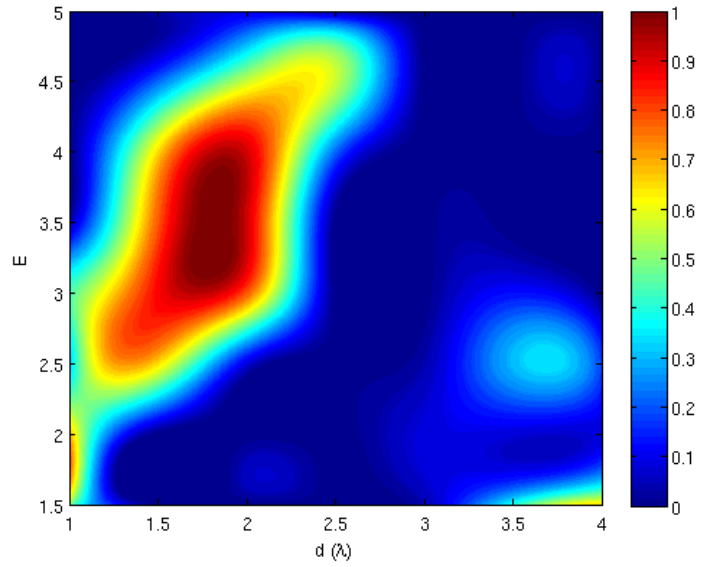
Figure 41. Contour map of success rates for corner reflector ($l = 0.5\ \lambda$).
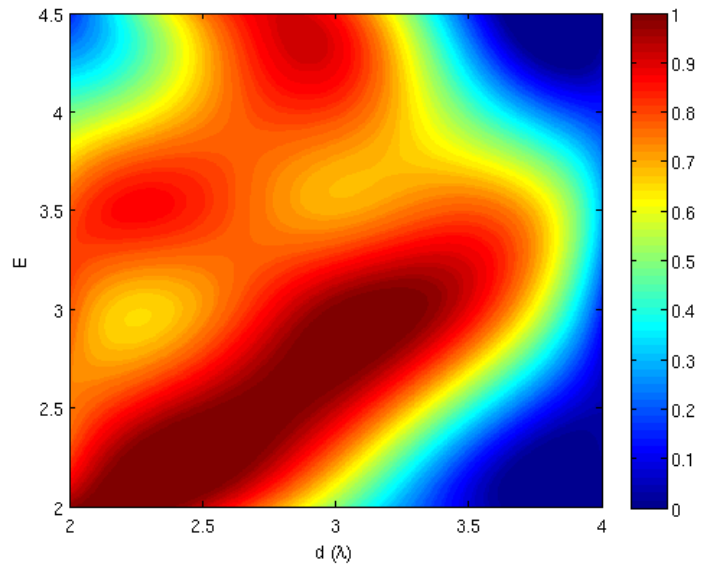


Figure 42. Contour map of success rates for corner reflector ($l = 1\ \lambda$).
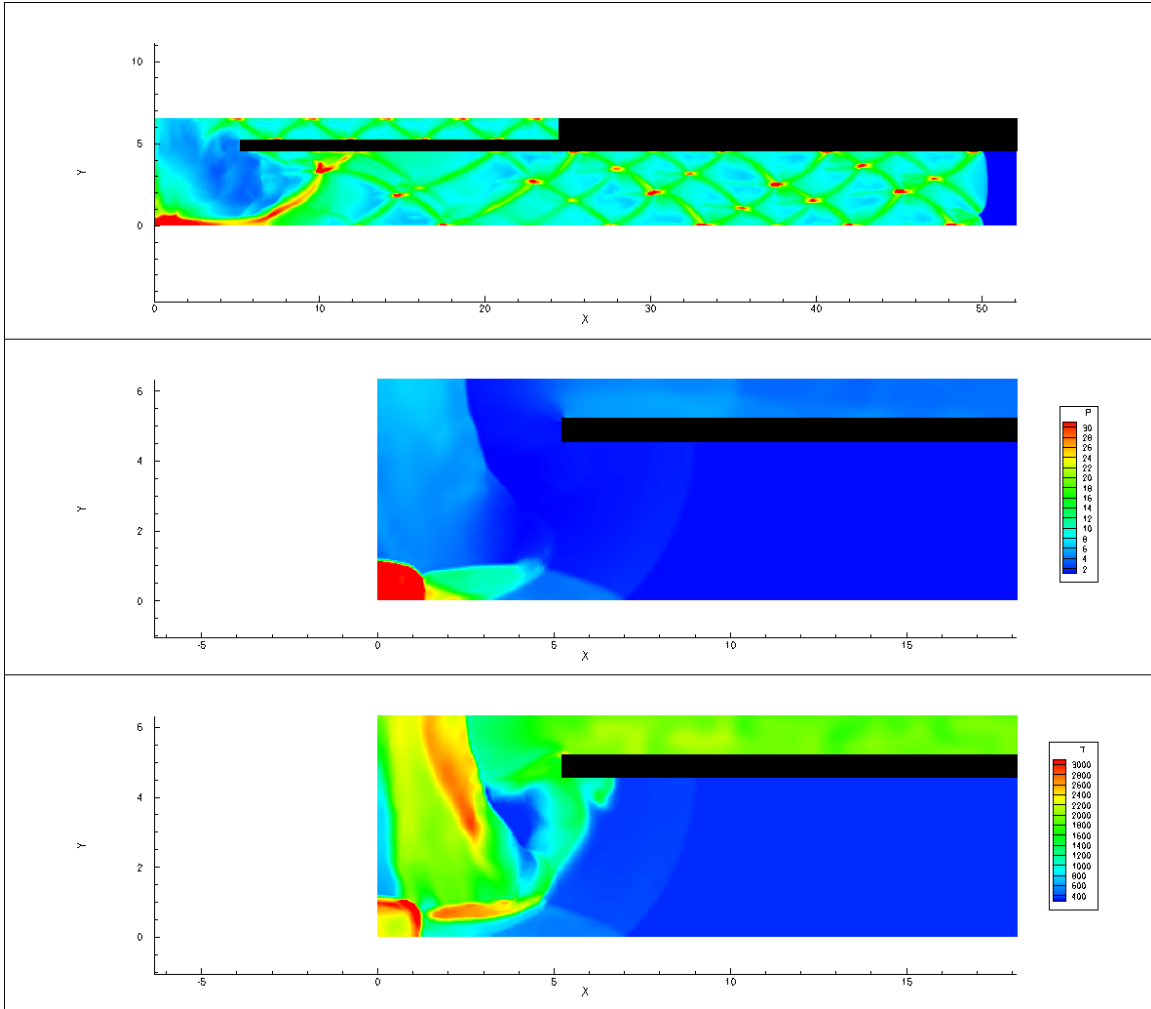
Figure 43. Successful transition for corner reflector with $l = 0.5$ $\lambda$, $E = 3.5$, and $d = 2$ $\lambda$ due to explosion at corner.

## Tables

Table 4. Success rates for symmetric step base cases (no obstruction).

|   |     | $E$ | | | | | | | | | |
|---|-----|------|------|------|------|------|------|------|------|------|------|
|   |     | 1.5  | 2    | 2.5  | 3    | 3.5  | 4    | 4.5  | 5    | 5.5  | 6    |
| $l$ | 1   | 0.34 | 0.06 | 0.13 | 0.02 | -    | -    | -    | -    | -    | -    |
|   | 1.5 | 0.74 | 0.53 | 0.05 | 0.03 | -    | -    | -    | -    | -    | -    |
|   | 2   | 1.00 | 0.44 | 0.56 | 0.83 | 0.61 | 0.67 | 0.67 | 0.67 | 0.56 | 0.28 |
|   | 2.5 | 1.00 | 1.00 | 1.00 | 1.00 | 0.96 | 0.83 | 0.96 | 0.96 | 0.78 | 0.70 |

Table 5. Success rates for symmetric step ($l = 1\ \lambda$, $E = 1.5$) with flat plate.

|   |      | $d$ | | | | | | |
|---|------|------|------|------|------|------|------|------|
|   |      | 1    | 1.5  | 2    | 2.5  | 3    | 3.5  | 4    |
| $h$ | 0.25 | 0.36 | 0.34 | 0.85 | 0.79 | 0.64 | 0.36 | 0.43 |
|   | 0.5  | 0.02 | 0.13 | 0.68 | 0.89 | 0.96 | 0.74 | 0.85 |
|   | 0.75 | 0.00 | 0.09 | 0.45 | 0.85 | 0.83 | 0.79 | 0.62 |
|   | 1    | 0.00 | 0.00 | 0.00 | 0.23 | 0.26 | 0.23 | 0.00 |

Table 6. Success rates for symmetric step ($l = 1\ \lambda$, $E = 2$) with flat plate.

|   |      | $d$ | | | | | | |
|---|------|------|------|------|------|------|------|------|
|   |      | 1    | 1.5  | 2    | 2.5  | 3    | 3.5  | 4    |
| $h$ | 0.5  | 0.11 | 0.19 | 0.04 | 0.43 | 0.49 | 0.43 | 0.40 |
|   | 0.75 | 0.00 | 0.17 | 0.00 | 0.45 | 0.64 | 1.00 | 0.57 |
|   | 1    | 0.00 | 0.06 | 0.00 | 0.02 | 0.55 | 0.74 | 0.5. |

Table 7. Success rates for symmetric step ($l = 1\ \lambda$, $E = 2.5$) with flat plate.

|   |      | $d$ | | | | | | | | |
|---|------|------|------|------|------|------|------|------|------|------|
|   |      | 1    | 1.5  | 2    | 2.5  | 3    | 3.5  | 4    | 4.5  | 5    |
|   | 0.5  | 0.04 | 0.11 | 0.09 | 0.04 | 0.15 | 0.17 | 0.13 | 0.09 | 0.09 |
|   | 0.75 | 0.00 | 0.09 | 0.00 | 0.00 | 0.15 | 0.17 | 0.21 | 0.21 | 0.49 |
| $h$ | 1    | 0.00 | 0.11 | 0.00 | 0.00 | 0.17 | 0.19 | 0.19 | 0.47 | 0.57 |
|   | 1.25 | 0.00 | 0.06 | 0.00 | 0.00 | 0.00 | 0.11 | 0.15 | 0.60 | 0.51 |
|   | 1.5  | 0.00 | 0.00 | 0.00 | 0.00 | 0.00 | 0.00 | 0.00 | 0.06 | 0.04 |

Table 8. Success rates for symmetric step ($l = 1.5\ \lambda$, $E = 1.5$) with flat plate.

| | | | | | $d$ | | | |
|---|---|---|---|---|---|---|---|---|
| | | 1 | 1.5 | 2 | 2.5 | 3 | 3.5 | 4 |
| | 0.15 | 0.68 | 0.74 | 0.74 | 0.74 | 0.74 | 0.82 | 0.82 |
| | 0.25 | 0.68 | 0.74 | 0.74 | 0.76 | 0.87 | 0.95 | 0.87 |
| $h$ | 0.5 | 0.63 | 0.76 | 0.61 | 0.58 | 0.66 | 0.58 | 0.68 |
| | 1 | 0.26 | 0.50 | 0.42 | 0.29 | 0.24 | 0.39 | 0.84 |
| | 1.5 | 0.00 | 0.00 | 0.00 | 0.00 | 0.03 | 0.00 | 0.18 |

Table 9. Success rates for symmetric step ($l = 1.5\ \lambda$, $E = 2$) with flat plate.

| | | | | $d$ | | | |
|---|---|---|---|---|---|---|---|
| | | 1 | 1.5 | 2 | 2.5 | 3 | 3.5 |
| | 0.5 | 0.47 | 0.55 | 0.53 | 0.50 | 0.47 | 0.42 |
| | 1 | 0.26 | 0.53 | 0.53 | 0.32 | 0.08 | 0.26 |
| $h$ | 1.5 | 0.00 | 0.21 | 0.68 | 0.26 | 0.00 | 0.13 |
| | 2 | 0.00 | 0.00 | 0.05 | 0.00 | 0.00 | 0.00 |
| | 2.5 | 0.00 | 0.00 | 0.00 | 0.00 | 0.00 | 0.00 |

Table 10. Success rates for symmetric step ($l = 1.5\ \lambda$, $E = 2.5$) with flat plate.

| | | | | $d$ | | | |
|---|---|---|---|---|---|---|---|
| | | 1 | 1.5 | 2 | 2.5 | 3 | |
| | 0.5 | 0.18 | 0.26 | 0.13 | 0.08 | 0.05 | 0.05 |
| | 1 | 0.03 | 0.47 | 0.37 | 0.11 | 0.05 | 0.00 |
| $h$ | 1.5 | 0.00 | 0.16 | 0.47 | 0.29 | 0.00 | 0.00 |
| | 2 | 0.00 | 0.00 | 0.39 | 0.26 | 0.00 | 0.00 |
| | 2.5 | 0.00 | 0.00 | 0.00 | 0.05 | 0.00 | 0.00 |

Table 11. Success rates for symmetric step ($l = 1.5\ \lambda$, $E = 3$) with flat plate.

| | | | | $d$ | | | |
|---|---|---|---|---|---|---|---|
| | | 1 | 1.5 | 2 | 2.5 | 3 | 3.5 |
| | 0.5 | 0.05 | 0.08 | 0.03 | 0.03 | 0.03 | 0.03 |
| | 1 | 0.03 | 0.05 | 0.05 | 0.03 | 0.00 | 0.00 |
| $h$ | 1.5 | 0.03 | 0.00 | 0.16 | 0.11 | 0.00 | |
| | 2 | 0.00 | 0.00 | 0.32 | 0.13 | 0.00 | 0.00 |
| | 2.5 | 0.00 | 0.00 | 0.00 | 0.16 | 0.00 | 0.00 |

Table 12. Success rates for symmetric step ($l = 2\ \lambda$, $E = 2$) with flat plate.

|   |     | $d$ |
|---|-----|------|------|------|------|
|   |     | 1    | 2    | 3    | 4    |
|   | 0.5 | 0.44 | 0.67 | 0.44 | 0.44 |
| $h$ | 1   | 0.22 | 1.00 | 0.44 | 0.11 |
|   | 1.5 | 0.22 | 1.00 | 0.39 | 0.06 |
|   | 2   | 0.00 | 0.83 | 0.39 | 0.00 |

Table 13. Success rates for symmetric step ($l = 2\ \lambda$, $E = 3$) with flat plate.

|   |     | $d$ |
|---|-----|------|------|------|------|
|   |     | 1    | 2    | 3    | 4    |
|   | 0.5 | 0.00 | 0.78 | 0.83 | 0.83 |
|   | 1   | 0.00 | 0.78 | 0.83 | 0.28 |
|   | 1.5 | 0.83 | 0.78 | 0.83 | 0.00 |
| $h$ | 2   | 1.00 | 0.61 | 0.72 | 0.00 |
|   | 2.5 | 1.00 | 0.17 | 0.89 | 0.00 |
|   | 3   | 0.39 | 0.11 | 0.61 | 0.00 |

Table 14. Success rates for symmetric step ($l = 2\ \lambda$, $E = 4$) with flat plate.

|   |     | $d$ |
|---|-----|------|------|------|------|
|   |     | 1    | 2    | 3    | 4    |
|   | 0.5 | 0.00 | 0.61 | 0.67 | 0.56 |
|   | 1   | 0.00 | 0.50 | 0.83 | 0.56 |
|   | 1.5 | 1.00 | 0.67 | 0.72 | 0.44 |
| $h$ | 2   | 1.00 | 0.56 | 0.50 | 0.28 |
|   | 2.5 | 1.00 | 0.83 | 0.39 | 0.44 |
|   | 3   | 0.83 | 0.78 | 0.67 | 0.33 |

Table 15. Success rates for symmetric step ($l = 2\ \lambda$, $E = 5$) with flat plate.

|   |     | $d$ |
|---|-----|------|------|------|------|
|   |     | 1    | 2    | 3    | 4    |
|   | 0.5 | 0.00 | 0.61 | 0.56 | 0.39 |
|   | 1   | 0.00 | 0.28 | 0.44 | 0.50 |
|   | 1.5 | 0.00 | 0.33 | 0.50 | 0.39 |
| $h$ | 2   | 0.00 | 0.72 | 0.50 | 0.39 |
|   | 2.5 | 0.00 | 1.00 | 0.50 | 0.28 |
|   | 3   | 0.78 | 1.00 | 0.56 | 0.44 |

61

Table 16. Success rates for corner reflector ($l = 0.5\ \lambda$).

| | | $d$ | | | | | | |
|---|---|---|---|---|---|---|---|---|
| | | 1 | 1.5 | 2 | 2.5 | 3 | 3.5 | 4 |
| | 1.5 | 0.48 | 0.00 | 0.00 | 0.00 | 0.04 | 0.39 | 0.65 |
| | 2 | 0.70 | 0.00 | 0.00 | 0.00 | 0.09 | 0.09 | 0.09 |
| | 2.5 | 0.30 | 0.65 | 0.09 | 0.00 | 0.04 | 0.30 | 0.17 |
| $E$ | 3 | 0.43 | 0.87 | 0.78 | 0.00 | 0.00 | 0.13 | 0.00 |
| | 3.5 | 0.04 | 0.78 | 0.91 | 0.00 | 0.00 | 0.00 | 0.00 |
| | 4 | 0.00 | 0.65 | 0.91 | 0.21 | 0.00 | 0.00 | 0.00 |
| | 4.5 | 0.00 | 0.22 | 0.57 | 0.57 | 0.00 | 0.00 | 0.00 |
| | 5 | 0.00 | 0.04 | 0.09 | 0.00 | 0.00 | 0.00 | 0.00 |

Table 17. Success rates for corner reflector ($l = 1\ \lambda$).

| | | $d$ | | | | |
|---|---|---|---|---|---|---|
| | | 2 | 2.5 | 3 | 3.5 | 4 |
| | 2 | 0.98 | 0.94 | 0.51 | 0.09 | 0.00 |
| | 2.5 | 0.74 | 0.98 | 0.94 | 0.43 | 0.04 |
| $E$ | 3 | 0.79 | 0.72 | 1.00 | 0.89 | 0.15 |
| | 3.5 | 0.79 | 0.83 | 0.70 | 0.79 | 0.30 |
| | 4 | 0.49 | 0.72 | 0.81 | 0.47 | 0.15 |
| | 4.5 | 0.15 | 0.74 | 0.85 | 0.17 | 0.00 |

# Bibliography

1. Strehlow, R. A., 1984. *Combustion Fundamentals* McGraw-Hill Book Company, New York.

2. Glassman, I., 1996. *Combustion*, third ed. Academic Press, San Diego.

3. Kuo, K., 1986. *Principles of Combusion* John Wiley & Sons, New York.

4. Schauer, F., Stutrud, J., and Bradley, R., 2001. "Detonation Initiation Studies and Performance Results for Pulsed Detonation Engine Applications." In 39th AIAA Aerospace Sciences Meeting & Exhibit, AIAA.

5. Hopper, D. R., King, P. I., Schauer, F. R., Katta, V. R., and Hoke, J. L., 2007. "Detonation Propagation across an Asymmetric Step Expansion." In 43rd AIAA/ASME/SAE/ASEE Joint Propulsion Conference & Exhibit, AIAA.

6. Hoke, J. L., Bradley, R. P., Gallia, J. R., and Schauer, F. R., 2006. "The Impact of Detonation Initiation Techniques on Thrust in a Pulsed Detonation Engine." In 44th AIAA Aerospace Sciences Meeting and Exhibit, AIAA.

7. Hoke, J. L., Bradley, R. P., and Schauer, F. R., 2005. "Impact of DDT Mechanism, Combustion Wave Speed, Temperature, and Charge Quality on Pulsed-Detonation-Engine Performance." In 43rd AIAA Aerospace Sciences Meeting, AIAA.

8. Katta, V. R., 2008. "Asymmetric Expansion of detonation Wave in an Array of Tubes." In 44th AIAA/ASME/SAE/ASEE Joint Propulsion Conference & Exhibit, AIAA.

9. Thomas, G. O., Edwards, D. H., Lee, J. H., Knystautas, R., Moen, I. O., and Wei, Y. M., 1986. "Detonation Diffraction by Divergent Channels." *Progress in Astronautics and Aeronautics,* **106**, pp. 144–154.

10. Pantow, E., Fisher, M., and Kratzel, T., 1996. "Decoupling and recoupling of detonation waves associated with sudden expansion." *Shock Waves*, pp. 131–137.

11. Schultz, E., and Shepherd, J., 2000. Detonation Diffraction Through a Mixture Gradient. Explosion dynamics laboratory report fm00-1, California Institute of Technology.

12. Saretto, S. R., Lee, S. Y., Conrad, C., Brumberg, J., Pal, S., and Santoro, R. J. "Predetonator To Thrust Tube Detonation Transition Studies For Mult-cycle PDE Applications.".

13. Moen, I. O., Sulmistras, A., Thomas, G. O., Bjerketvedt, D., and Thibault, P. A., 1986. "Influence of Cellular Regularity on the Behavior of Gaseous Detonations." *Progress in Astronautics and Aeronautics,* **106**, pp. 220–243.

14. Jackson, S. I., and Shepherd, J. E., 2002. "Initiation Systems For Pulse Detonation Engines." In 38th AIAA/ASME/SAE/ASEE Joint Propulsion Conference and Exhibit, AIAA.

15. Turns, S. R., 2000. *An Introduction to Combustion*, second ed. McGraw-Hill Book Company, New York.

16. Kao, S., and Shepherd, J. E., 2004. Numerical Solution Methods for Control Volume Explosions and ZND Detonation Structure. Galcit report fm2006.007, California Institute of Technology.

17. Katta, V. R., Chin, L. P., and Schauer, F., 1999. "Numerical Studies on Cellular Detonation Wave Subjected to Sudden Expansion." In Proceedings of the 17th International Colloquium on the Dynamics of Explosions and Reactive Sytems.

18. Korobeinikov, V. P., Levin, V. A., Markov, V. V., and Chernyi, G. G., 1972. "Propagation of Blast Waves in a Combustible Gas." *Astronautica Acta,* **17**(4 & 5), pp. 529–536.

19. MacCormack, R. W., 1969. "The Effect Of Viscosity In Hypervelocity Impact Cratering." *Journal of Spacecraft and Rockets,* **40**(5), pp. 757–763.

20. Boris, J. P., and Book, D. L., 1973. "Flux-Corrected Transport. I. SHASTA, A Fluid Transport Algorithm That Works." *Journal of Computational Physics,* **11**, pp. 38–69.

21. Finlayson, B. A., 1992. *Numerical Methods for Problems with Moving Fronts* Ravenna Park Publishing, Inc., Seattle.

22. Hirsch, C., 2007. *Numerical Computation of Internal & External Flows*, second ed. Elsevier, Oxford.

# Vita

Second Lieutenant Fievisohn graduated high school in 2004 and attended Clarkson University in New York. He graduated in 2008 with a degree in Aeronautical Engineering and a second degree in Applied Mathematics and Statistics. After graduation he was assigned to attend AFIT in August 2008. He compled the Aeronautical Engineering program in March 2010. His next assignment is to the Air Force Research Labs at Wright-Patterson AFB. He will be working for the Air Vehicles Directorate.

| REPORT DOCUMENTATION PAGE | | | | *Form Approved* <br> *OMB No. 0704–0188* |
|---|---|---|---|---|

The public reporting burden for this collection of information is estimated to average 1 hour per response, including the time for reviewing instructions, searching existing data sources, gathering and maintaining the data needed, and completing and reviewing the collection of information. Send comments regarding this burden estimate or any other aspect of this collection of information, including suggestions for reducing this burden to Department of Defense, Washington Headquarters Services, Directorate for Information Operations and Reports (0704–0188), 1215 Jefferson Davis Highway, Suite 1204, Arlington, VA 22202–4302. Respondents should be aware that notwithstanding any other provision of law, no person shall be subject to any penalty for failing to comply with a collection of information if it does not display a currently valid OMB control number. PLEASE DO NOT RETURN YOUR FORM TO THE ABOVE ADDRESS.

| 1. REPORT DATE (DD–MM–YYYY) <br> March 25 2010 | 2. REPORT TYPE <br> Master's Thesis | 3. DATES COVERED (*From — To*) <br> August 2008 – March 2010 |
|---|---|---|

| 4. TITLE AND SUBTITLE <br> Numerical Investigation of Pre-detonator Geometries for PDE Applications | 5a. CONTRACT NUMBER |
|---|---|
| | 5b. GRANT NUMBER |
| | 5c. PROGRAM ELEMENT NUMBER |
| 6. AUTHOR(S) <br><br> Fievisohn, Robert T., 2LT, USAF | 5d. PROJECT NUMBER |
| | 5e. TASK NUMBER |
| | 5f. WORK UNIT NUMBER |

| 7. PERFORMING ORGANIZATION NAME(S) AND ADDRESS(ES) <br> Air Force Institute of Technology <br> Graduate School of Engineering and Management (AFIT/ENY) <br> 2950 Hobson Way <br> WPAFB OH 45433-7765 | 8. PERFORMING ORGANIZATION REPORT NUMBER <br><br> AFIT/GAE/ENY/10-M09 |
|---|---|
| 9. SPONSORING / MONITORING AGENCY NAME(S) AND ADDRESS(ES) <br> AFRL/RZTC – Dr. Frederick Schauer <br> (Frederick.schauer@wpafb.af.mil) <br> Building 490 Room 112 <br> WPAFB, OH 45433 <br> (937) 255-6462 | 10. SPONSOR/MONITOR'S ACRONYM(S) |
| | 11. SPONSOR/MONITOR'S REPORT NUMBER(S) |

12. DISTRIBUTION / AVAILABILITY STATEMENT
APPROVED FOR PUBLIC RELEASE; DISTRIBUTION UNLIMITED

13. SUPPLEMENTARY NOTES

14. ABSTRACT
A parametric study was performed to determine optimal geometries to allow the successful transition of a detonation from a pre-detonator into the thrust tube of a pulse detonation engine. The study was performed using a two-dimensional Euler solver with progress variables to model the chemistry. The geometrical configurations for the simulations look at the effect of shock reflections, flow obstructions, and detonation diffraction to determine successful geometries. It was observed that there are success and failure rates associated with pre-detonators. These success rates appear to be determined by the transverse wave structure of a stably propagating detonation wave and must be considered in the design and testing of a practical pre-detonator. A simple and straight forward method of estimating the success rate is presented. Desirable effects from geometries with high success rates are used as a basis for recommendations for future pre-detonator designs.

15. SUBJECT TERMS
detonation, PDE, pre-detonator, CFD, success rate, thrust tube, parametric study

| 16. SECURITY CLASSIFICATION OF: | | | 17. LIMITATION OF ABSTRACT | 18. NUMBER OF PAGES | 19a. NAME OF RESPONSIBLE PERSON <br> Dr. Paul King, AFIT/ENY |
|---|---|---|---|---|---|
| a. REPORT | b. ABSTRACT | c. THIS PAGE | UU | 80 | 19b. TELEPHONE NUMBER (Include Area Code) <br> (937)255-3636, ext 4628 |
| U | U | U | | | |

**Standard Form 298 (Rev. 8–98)**
*Prescribed by ANSI Std. Z39.18*